

1 **The Aare main overdeepening on the northern margin of the European Alps: Basins, riegels,**  
2 **and slot canyons**

3  
4 Fritz Schlunegger<sup>1</sup>, Edi Kissling<sup>2</sup>, Dimitri Bandou<sup>1,3</sup>, Guilhem Douillet<sup>1</sup>, David Mair<sup>1</sup>, Urs Marti<sup>4</sup>,  
5 Regina Reber<sup>1</sup>, Patrick Schläfli<sup>1,5</sup>, and Michael Schwenk<sup>1,6</sup>

6  
7 <sup>1</sup>Institute of Geological Sciences, University of Bern, Baltzerstrasse 1+3, 3012 Bern, Switzerland

8 <sup>2</sup>Department of Earth Sciences, ETH Zürich, Sonneggstrasse 5, 8092 Zürich, Switzerland

9 <sup>3</sup>Department of Environmental Sciences, University of Virginia, 291 McCormick Rd., Charlottesville,  
10 VA 22904-4123, USA

11 <sup>4</sup>Landesgeologie Swisstopo, Seftigenstrasse 264, Postfach, 3084 Wabern, Switzerland

12 <sup>5</sup>Institute of Plant Sciences and Oeschger Centre for Climate Change Research, Altenbergrain 21,  
13 3013 Bern, Switzerland

14 <sup>6</sup>Bayerisches Landesamt für Umwelt, Umweltdienstleistungen, Hof, 95030 Hof Saale, Germany

15  
16 [fritz.schlunegger@unibe.ch](mailto:fritz.schlunegger@unibe.ch)

17  
18 **Abstract**

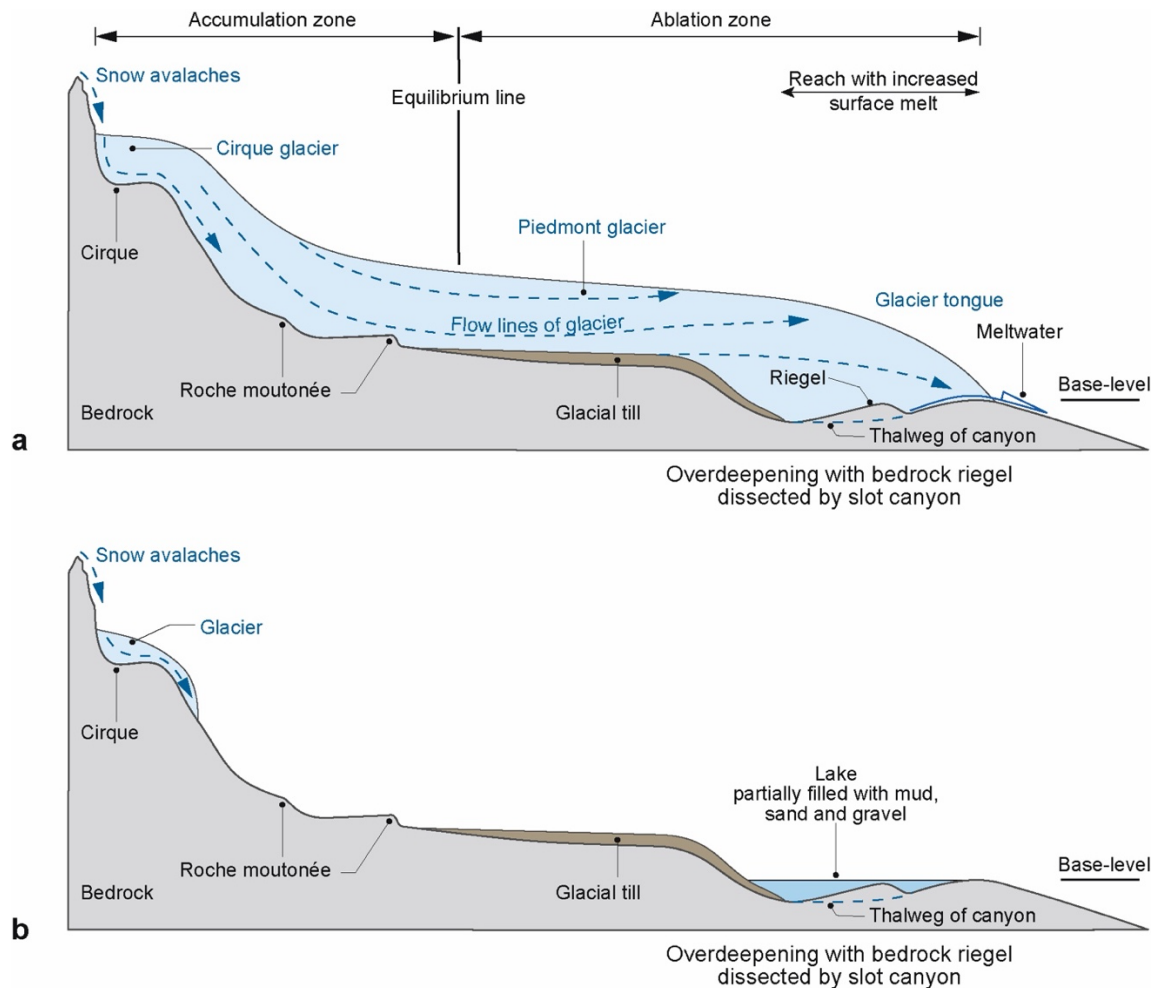
19 This work summarizes the results of an interdisciplinary project where we aimed to explore the origin  
20 of overdeepenings through a combination of a gravimetry survey, drillings and dating. To this end, we  
21 focused on the Bern area, Switzerland, situated on the northern margin of the European Alps. This area  
22 experienced multiple advances of piedmont glaciers during the Quaternary glaciations, resulting in the  
23 carving of the main overdeepening of the Aare River valley (referred to as the Aare main  
24 overdeepening). This bedrock depression is tens of km long and up to several hundreds of m to a few  
25 km wide. We found that in the Bern area, the Aare main overdeepening is made up of two >200 m-deep  
26 troughs that are separated by a c. 5 km-long and up to 150 m-high transverse rocky ridge, interpreted  
27 as a riegel. The basins and the riegel are overlain by a >200 m- and a c. 100 m-thick succession of  
28 Quaternary sediments, respectively. The bedrock itself is made up of a Late Oligocene to Early Miocene  
29 suite of consolidated clastic deposits, which are part of the Molasse foreland basin. In contrast, the  
30 Quaternary suite comprises a middle Pleistocene to Holocene succession of unconsolidated glacio-  
31 lacustrine gravel, sand and mud. A synthesis of published gravimetry data revealed that the upstream  
32 stoss side of the bedrock riegel is c. 50% flatter than the downstream lee side. In addition, information  
33 from >100 deep drillings reaching depths >50 m suggests that the bedrock riegel is dissected by an  
34 anastomosing network of slot canyons. Apparently, the slot canyons established the hydrological  
35 connection between the upstream and downstream basins during their formation. Based on published  
36 modelling results, we interpret that the riegels and canyons were formed through incision of subglacial

37 meltwater during a glacier's decay state, when large volumes of meltwater were released. It appears  
38 that such a situation has repeatedly occurred since the Middle Pleistocene Transition approximately 800  
39 ka ago, when large, several hundreds of m-thick and erosive piedmont glaciers began to advance far  
40 into the foreland. This resulted in the deep carving of the inner-Alpine valleys and additionally in the  
41 formation of overdeepenings, riegels and slot canyons on the plateau situated on the northern margin of  
42 the Alps.

43

## 44 **1 Introduction**

45 Overdeepenings are bedrock depressions below the current fluvial base-level (e.g., Jørgensen and  
46 Sandersen, 2006; Dürst Stucki et al., 2010; 2013; Fischer and Häberli, 2012). The downstream closures  
47 of these basins have adverse slopes that generally dip in the upstream direction (Häberli et al., 2016).  
48 Because bedrock depressions with such characteristics (Figure 1) are commonly found in previously  
49 glaciated areas, their formation has been interpreted as resulting from the erosional work of glaciers  
50 and/or subglacial meltwater (Wright, 1973; Herman and Braun, 2008; Egholm et al., 2009; Kehew et  
51 al., 2012; Patton et al., 2016; Liebl et al., 2023; and many others). Overdeepenings have been reported  
52 for the Quaternary from beneath the Greenland and Antarctic glaciers (Ross et al., 2011; Patton et al.,  
53 2016), but also in the North Sea (Moreau et al., 2012, Lohrberg et al., 2022), North America (Wright,  
54 1973; Lloyd et al., 2023) and northern Europe including Scandinavia (Clark and Walder, 1994;  
55 Piotrowski, 1997; Krohn et al., 2009). Glaciogenic paleovalleys are not only limited to the Quaternary  
56 but were also described for Paleozoic glaciations (e.g. Douillet et al., 2012; Dietrich et al., 2021). In the  
57 European Alps, such erosional troughs occur in Alpine valleys as well as on foreland plateaus on either  
58 side of this mountain belt (Preusser et al., 2010; Dürst Stucki and Schlunegger, 2013; Magrani et al.,  
59 2020). Pollen analysis (Welten, 1982; 1988; Schlüchter, 1989; Schläfli et al., 2021), dating using  
60 optically stimulating luminescence methods (Preusser et al., 2005; Dehnert et al., 2012; Büchi et al.,  
61 2018; Schwenk et al., 2022a) and  $^{14}\text{C}$  ages established on organic matter encountered in the  
62 overdeepening fill (Kellerhals and Häfeli, 1984) showed that these troughs were formed after the Middle  
63 Pleistocene Transition, which occurred c. 800 ka ago (Schlüchter, 2004). Geophysical surveys (e.g.,  
64 Rosselli and Raymond, 2003; Reitner et al., 2010; Stewart and Lonergan, 2011; Stewart et al., 2013;  
65 Perrouty et al., 2015; Burschil et al., 2018; 2019; Ottesen et al., 2020) in combination with drillings  
66 (Jordan, 2010; Dürst Stucki et al., 2010; Büchi et al., 2017; 2018; Gegg et al., 2021; Bandou et al., 2022;  
67 2023; Anselmetti et al., 2022; Schwenk et al., 2022a, b; Gegg and Preusser, 2023; Schaller et al., 2023)  
68 disclosed that such overdeepenings can be several km wide, tens of km long and >200 m deep. The  
69 surveys also showed that overdeepenings are typically composed of individual sub-basins, separated by  
70 bedrock swells or bumps oriented transverse to the flow of a former glacier, hereafter called riegels  
71 (Cook and Swift, 2012), yet the specific details of such a geometry have not yet been elaborated.



72

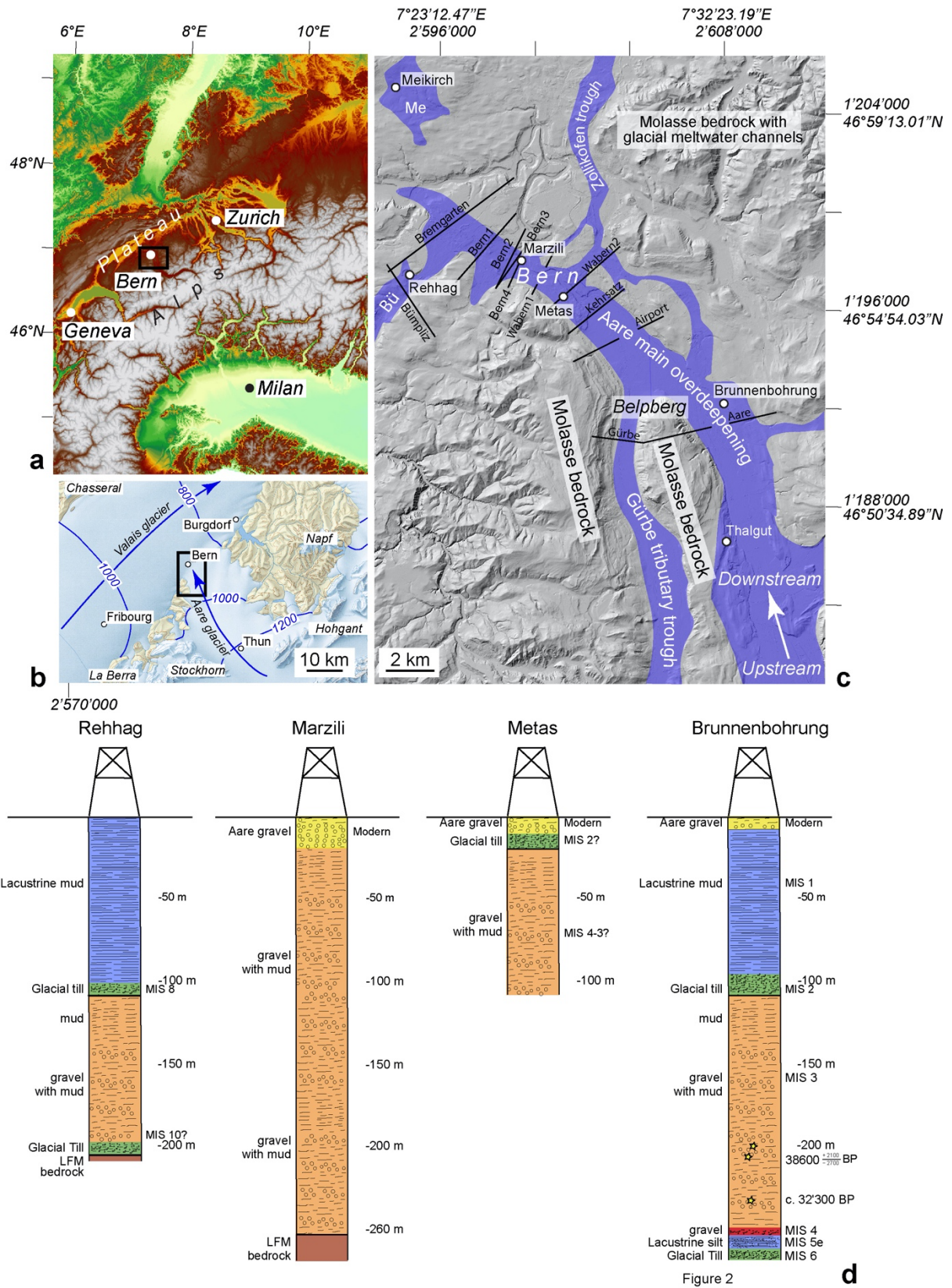
Figure 1

Figure 1: Architecture of a landscape sculpted by piedmont glaciers during glaciations. a) Situation immediately following a full glacial period during which a piedmont glacier, which extended far into the foreland, started to melt. As a result, large volumes of meltwater are produced in the ablation zone close to the glacier's tongue. This meltwater has the potential to contribute to the erosional downwearing of the bedrock, and it can cause the incision of canyons into bedrock riegels, which separate two overdeepened basins. b) During interglacial time periods, the piedmont glaciers disappear, and small ice caps may be preserved in the higher parts of a mountain belt. During this time, the overdeepened basin will be filled by lacustrine sediments and/or will eventually host a lake. Modified after Schlunegger and Garefalakis (2023).

73

74 Here, we summarize the results of an interdisciplinary project where we aim to explore the origin of  
 75 overdeepenings using a combination of data collected through a gravimetry survey (Bandou, 2023a;  
 76 Bandou et al., 2022, 2023), drillings (Reber and Schlunegger, 2016; Schwenk et al., 2022a, b) and  
 77 dating (Schläfli et al., 2021; Schwenk et al., 2022a). We focus our study on the Bern area situated on  
 78 the northern margin of the European Alps (Figure 2). For this region, we draw a map of the bedrock  
 79 topography combining the results of a gravimetry survey in the region (Bandou, 2023a; Bandou et al.,  
 80 2023) with information obtained through drillings. This map shows that an overdeepened trough or a  
 81 tunnel valley system, referred to as the Aare main overdeepening (Schwenk et al., 2022a), is made up  
 82 of two basins separated by a bedrock riegel, which itself is cut by one or multiple slot canyons. This

83 structure has a similar geometry as many examples reported from formerly glaciated landscapes  
 84 (Brocklehurst and Whipple, 2002; Brocklehurst et al., 2008) and particularly from Alpine valleys,  
 85 which points to similar processes resulting in their formation.



86

Figure 2: Local setting illustrating the a) Alpine arc (modified from Bandou et al., 2023) with latitudes and longitudes, b) the study area during the Last Glacial Maximum (LGM; map with isohypses of the glacier's surfaces taken from Bini et al., 2009), c) the surface geomorphology (2 m-SwissAlti3D DEM © swisstopo) together with the orientation of the Aare main overdeepening, taken from Reber and Schlunegger (2016), and d) information from drillings. The figure c) shows (i) the sections along which gravity data was collected (black lines; Bandou et al., 2022; 2023), and (ii) the sites (white circles) where sediments in drillings (Rehag: Schwenk et al., 2022a, b; Meikirch: Welten, 1982; Preusser et al., 2005; Schläfli et al., 2021; Brunnenbohrung: Kellerhals and Häfeli, 1984; Zwahlen et al., 2021) and exposures (Thalgut: Welten, 1982; 1988; Schlüchter, 1989; Preusser and Schlüchter, 2004) were either dated with various techniques, or where existing ages were reconfirmed by a subsequent analysis. Me=Meikirch overdeepening; Bü=Bümpliz trough. The numbers along the figure margin refer to the Swiss coordinate system (CH1903+) and are complemented with information on latitudes and longitudes. Panel d) presents the logs of key drillings. The Brunnenbohrung drilling was reconstructed from cuttings; the material at Metas and Rehag was cored (Geotest, 1997; Schwenk et al., 2022a), whereas the sedimentary log of the Marzili drilling is based on a combination of cuttings and gamma ray data (Gees, 1974). The log of the Brunnenbohrung is taken from Bandou et al. (2022).

87

## 88 **2 Setting**

### 89 *2.1 Overdeepened troughs in the Bern area*

90 The target overdeepening near Bern was sculpted by the Aare piedmont glacier with sources in the  
 91 Central European Alps. From there, the Aare glacier flowed onto the Swiss Plateau (Figure 2a) over a  
 92 distance of >20 km, and it merged with the Valais glacier north of Bern, at least during the Last Glacial  
 93 Maximum (LGM) c. 20 ka ago (Figure 2b). Upstream of the city area of Bern, two bedrock depressions,  
 94 referred to as the Gürbe tributary trough and the Aare main overdeepening (Figure 2c), form prominent  
 95 basins. They are between c. 150 (Gürbe trough; Geotest, 1995) and >250 m deep (Aare main trough,  
 96 Kellerhals and Häfeli, 1984), and several km wide (Bandou et al., 2022). Downstream of the city of  
 97 Bern, the Aare main overdeepening splits into several distributary branches. Among these, the Bümpliz  
 98 trough ('Bü' in Figure 2c) is the most prominent one with a depth >200 m (Schwenk et al., 2022a, b).  
 99 The other depressions such as the Zollikofen trough are shallower and reach a depth of <150 m (Reber  
 100 and Schlunegger, 2016). The study region also hosts the Meikirch overdeepening (labelled as 'Me' on  
 101 Figure 3c), a nearly 200 m-deep trough (Dürst Stucki et al., 2010; Dürst Stucki and Schlunegger, 2003),  
 102 which appears to be isolated from the rest of the overdeepening system (Reber and Schlunegger, 2016).  
 103 Although the area between the northern termination of the Aare main overdeepening and the Meikirch  
 104 trough is made up of exposed bedrock (Gerber, 1927), the possibility of a connection between both  
 105 depressions via a narrow canyon, while quite unlikely according to Reber and Schlunegger (2016),  
 106 cannot be completely ruled out. The Aare main overdeepening itself is the most prominent trough in  
 107 the city area of Bern and has a maximum depth of nearly 250 m (Reber and Schlunegger, 2016).

108

### 109 *2.2 Chronologic framework of overdeepening fill*

110 The Quaternary fill of the Aare main overdeepening has been placed into the chronological framework  
 111 of glacial advances onto the Swiss plateau during the past glaciations by previous authors. South of  
 112 Bern, the Thalgut section (Figure 2c) disclosed the occurrence of pollen fragments embedded in a

113 lacustrine sequence at the base and near the top of the section (Schluchter, 1989). The pollen assemblage  
114 at the base was assigned to the Holsteinian interglacial period (Welten, 1982; 1988; Schluchter, 1989;  
115 Preusser and Schluchter, 2004), which either corresponds to MIS 9 (Roger et al., 1999) or MIS 11 (see  
116 discussion in Preusser et al., 2011; Koutsodendris et al., 2012; and Schwenk et al., 2022a for discussion  
117 of ages). The lacustrine sediments near the top of the same suite were assigned to MIS 5e (Welten,  
118 1982; 1988; Schluchter, 1989). Approximately 6 km farther downstream of the Thalgut section, the  
119 Brunnenbohrung drilling (Figure 2d) penetrated nearly the entire sedimentary sequence of the Aare  
120 main overdeepening. Based on lithostratigraphic constraints and <sup>14</sup>C ages established on organic  
121 fragments, Kellerhals and Häfeli (1984) and subsequently Zwahlen et al. (2021) assigned an age  
122 postdating MIS 6 to the entire succession. Farther north of Bern, Schwenk et al. (2022a) used the results  
123 of feldspar luminescence dating to propose that the sedimentary suite penetrated by the Rehlag drilling  
124 has an age of MIS 8 and older (Figure 2d). These ages are not precise enough to reconstruct in detail  
125 the history of how and when the overdeepenings were formed, but they are consistent with the view  
126 that the deep troughs in the Bern area were originally formed after the Middle Pleistocene Transition c.  
127 800 ka ago (Schluchter, 2004) and thus during the same period when the U-shaped Alpine valleys were  
128 carved (Häuselmann et al., 2007; Valla et al., 2011).

129

### 130 2.3 *Lithological architecture of bedrock*

131 The bedrock in the region comprises an amalgamated suite of Early Miocene Upper Marine Molasse  
132 (UMM) sandstone beds south of Bern. Sedimentological analyses showed that these sediments were  
133 deposited in a shallow marine, mostly coastal environment (Garefalakis and Schlunegger, 2019). In the  
134 region north of Bern, the bedrock is made up of a Late Oligocene to Early Miocene suite of Lower  
135 Freshwater Molasse (LFM) sandstones and mudstones (Isenschmid, 2019). These sediments were  
136 deposited in a fluvial environment comprising channel fills and floodplains made up of sandstones and  
137 mudstones, respectively (Platt and Keller, 1992; Isenschmid, 2019). The bedding of the sediments and  
138 the contact between the UMM and the LFM gently dips towards the south by c. 10° (Isenschmid, 2019),  
139 with the consequence that south of Bern, the base of the Aare main overdeepening often consists of  
140 LFM deposits, while most of the upper part of the overdeepening is laterally bordered by bedrock made  
141 up of UMM. In addition, it has been postulated that the UMM sediments have a lower erodibility than  
142 the underlying LFM unit, based on the observation that the UMM forms a cap rock in the region  
143 (Isenschmid, 2019). Finally, Isenschmid (2019) documented that the Molasse bedrock beneath the Bern  
144 city area is dissected by left-lateral faults that strike NW-SE, offering zones of mechanical weaknesses.

145

### 146 2.4 *Lithological architecture of overdeepening fill*

147 Detailed information on the lithologic architecture of the overdeepening fill is available from a few  
148 drillings only (Figure 2d). South of Bern, the >250 m-thick succession at the Brunnenbohrung site starts

149 with a few meters of till (possibly MIS 6), yet the drilling did not reach the bedrock. The till is overlain  
150 by a several m-thick lacustrine silt (possibly MIS 5e) and a >100 m-thick sequence made up of  
151 fluviolacustrine gravel, dated to MIS 3 based on <sup>14</sup>C concentrations in organic matter (Kellerhals and  
152 Häfeli, 1984). The topmost 100 m-thick suite comprises a till at its base (possibly MIS 2) and a  
153 monotonous succession of lacustrine mud topped by a fluvial gravel. Farther north, the Metas drilling  
154 penetrated a 110 m-thick sequence without reaching the bedrock (Geotest, 1997). It starts with a c. 90  
155 m-thick suite made up of mud and sand layers, which contain isolated clasts. These sediments were  
156 most likely deposited in a proglacial lake. It is overlain by a till (MIS 2?) and finally by a c. 15 m-thick  
157 proglacial gravel (Geotest, 1997). A similar sedimentologic architecture, based on cutting and gamma  
158 ray data, was also inferred for the Quaternary suite penetrated by the Marzili drilling situated in the city  
159 area of Bern (Gees, 1974). Finally, the Rehhag drilling, which was sunk into the Bümpliz tributary  
160 trough and which reached the bedrock (Schwenk et al., 2022a), unravelled a 210 m-thick succession of  
161 Quaternary sediments. The Quaternary suite starts with a few m-thick till, which is overlain by a c. 100  
162 m-thick sequence of mud, gravel and sand layers. A second till was identified at a drilling depth of 103  
163 m. It is overlain by a succession of mud with isolated pebbles, deposited in a proglacial lake. Apparently,  
164 the Quaternary successions are spatially highly heterogeneous as disclosed by the drillings, but they all  
165 record the same depositional setting as the sediments were most likely deposited in a glacio-lacustrine  
166 environment (e.g., Schwenk et al., 2022a).

167

## 168 2.5 *Density of Molasse bedrock and Quaternary sediments*

169 Data on the bulk density of the Molasse bedrock and the overlying Quaternary sediments is crucial for  
170 interpreting gravimetric datasets (Kissling and Schwendener, 1990). For the Bern region, Bandou et al.  
171 (2022) used the results of a Nettleton profile across the Belpberg mountain (that is underlain by Molasse  
172 bedrock, Figure 2c) to assign a bulk density of 2500 kg/m<sup>3</sup> to the Molasse units (Figure 2c). This is a  
173 substantially higher value than the bulk densities between 2150 and 2000 kg/m<sup>3</sup>, which have been  
174 determined for the basal part and the top sequences of the Quaternary suites in the Aare main  
175 overdeepening, respectively. These density values were measured with a multi sensor core logger on  
176 the core of the Rehhag drilling (Schwenk et al., 2022a) and obtained through 3D gravity modelling  
177 along several profiles in the Bern area (Bandou et al., 2022; 2023a). The results showed that the bulk  
178 densities of the Quaternary sediments depend less on the lithological architecture of the material or the  
179 depositional environment in which the sediments were deposited. Instead, they are primarily a function  
180 of the maximum depth of the overdeepening fill and the number of glaciations, during which the  
181 Quaternary sediments were compacted under a thick glacial cover (Bandou et al., 2023).

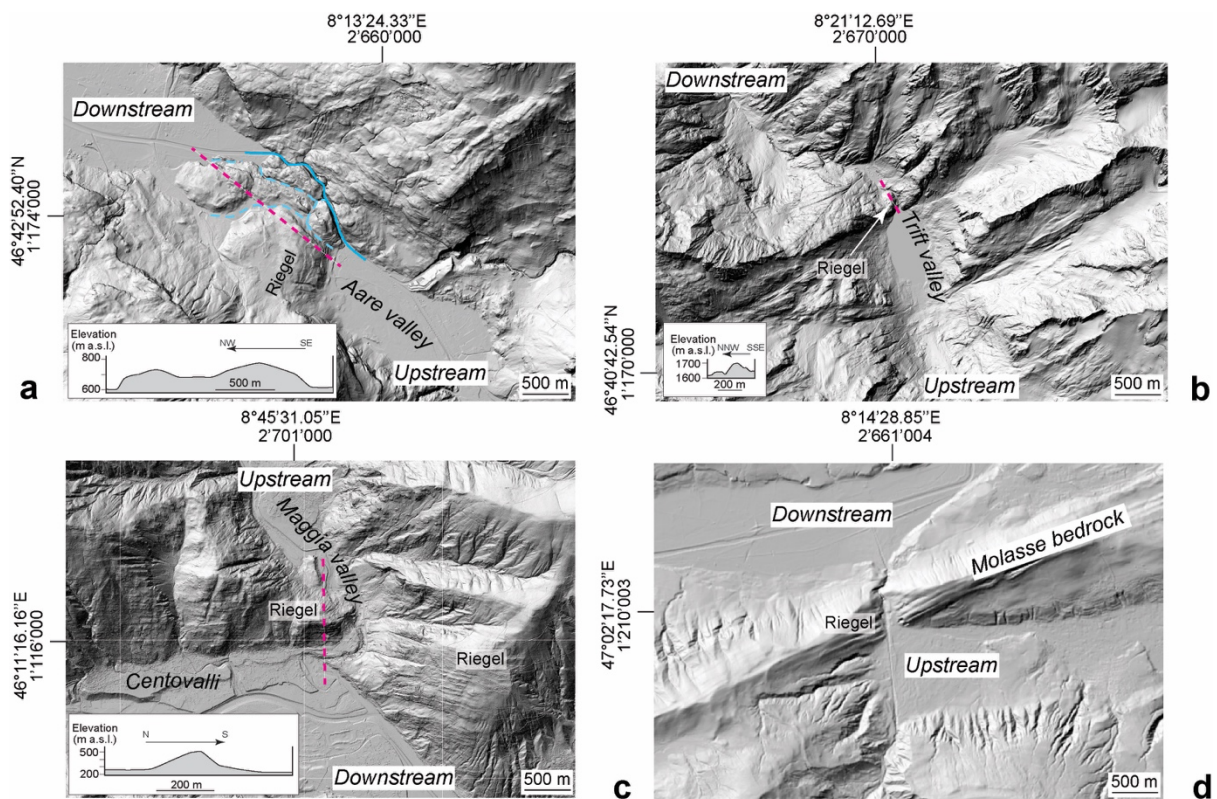
182

183

184

185 2.6 *Riegels and slot canyons in Alpine valleys*

186 Bedrock swells between neighbouring basins are common features in previously glaciated landscapes  
 187 (Anderson et al., 2006; Alley, 2019). They are common in the European Alps (see Figure 3, for a few  
 188 examples), and they have also been detected underneath active glaciers (Feiger et al., 2018; Nishiyama  
 189 et al., 2019). In the Alps, most of the bedrock swells cross the thalweg of valleys (Figure 3) and are  
 190 dissected by inner gorges or slot canyons that connect the upstream with the downstream basin (Hantke  
 191 and Scheidegger, 1973; Valla et al., 2010; Montgomery and Korup, 2011). In addition, Alpine bedrock  
 192 riegels have a geometry where the upstream stoss side is flatter than the downstream lee side (insets of  
 193 Figure 3). This is particularly the case for the swells in (Figure 3): the Aare valley (Figure 3a; dip of  
 194 stoss side and lee sides  $<5^\circ$  and  $>6^\circ$ , respectively; Hantke and Scheidegger, 1973), the Trift valley  
 195 (Figure 3b; c.  $30^\circ$  versus  $40^\circ$ ; Steinemann et al., 2021), and the Maggia valley (Figure 3c;  $6^\circ$  versus  
 196  $40^\circ$ ). Bedrock riegels and slot canyons are also found on the foreland plateau adjacent to the Alps such  
 197 as the example east of Lucerne (Figure 3d), yet their geometric expressions are less well-developed. In  
 198 this work, we will document that the overdeepening beneath the city of Bern shares the same geometric  
 199 properties as the ensemble of bedrock riegels and slot canyons in Alpine valleys.



200 Figure 3

Figure 3: Hillshade 2 m-SwissAlti3D DEM (© swisstopo) illustrating examples in Alpine valleys where bedrock riegels separate overdeepened basins situated farther upstream and downstream. The insets illustrate topographic sections across the riegels, and the arrows display the flow direction of the glaciers during a glaciation. The coordinates refer to the Swiss coordinate system (CH1903+). Longitudes and latitudes are also indicated.

201

### 202 3 Dataset and Methods

203 The bedrock topography beneath the city area of Bern was already reconstructed in 2010 and then  
204 updated in 2016, based on information from thousands of drillings publicly available on the Geoportal  
205 of the Canton Bern (see Dürst Stucki et al. (2010), and Reber and Schlunegger (2016), respectively).  
206 Since these drillings primarily penetrated the entire Quaternary sequence down to the bedrock at the  
207 lateral margins of the Aare main overdeepening, we consider the bedrock topography model of Reber  
208 and Schlunegger (2016) for the shallow parts of the trough as accurate. Yet detailed reconstructions of  
209 the deeper, central part of the overdeepening were hindered due to a lack of information from deep  
210 drillings at that time (Reber and Schlunegger, 2016). Here, we benefit from the results of a recent gravity  
211 survey conducted in the city area of Bern (Bandou et al., 2022; 2023; Bandou, 2023a) and information  
212 from new drillings >50 m deep. We proceeded through compiling, as a first step, the publicly available  
213 gravity data. We re-processed them to provide information about the spatial pattern of the gravity signal,  
214 either from the bedrock topography beneath the overdeepening fill (section 3.1) or from the  
215 overdeepening fill itself (section 3.2). Using these data along with the results from modelling conducted  
216 by Bandou et al. (2023), we reconstructed a map outlining the general thickness distribution of the  
217 Quaternary sediments (section 3.3). This was then used as the basis to update the existing bedrock  
218 topography model of Reber and Schlunegger (2016), thereby incorporating data from >100 drillings  
219 that penetrated >50 m into the subsurface (section 3.4).

220

#### 221 3.1 Assessing the gravity signal of the bedrock topography beneath the overdeepening

222 We compiled the gravity data collected by Bandou (2023a) and combined them with data archived in  
223 the Gravimetric Atlas of Switzerland by Swisstopo (Olivier et al., 2008; 2011). From this dataset, we  
224 calculated the Bouguer anomaly values (see Bandou et al., 2023, for references to the methodological  
225 papers) using the density of the Molasse bedrock ( $2500 \text{ kg/m}^3$ ) instead of the standard density of  $2670$   
226  $\text{kg/m}^3$  that is conventionally used for Bouguer anomaly corrections. We then draw the isogals (contour  
227 lines of equal Bouguer anomaly values) using the Golden Software Surface licensed to Swisstopo. This  
228 map was used to infer the general shape of the bedrock topography beneath the overdeepening fill. In  
229 particular, deviations of the isogals from the long-wavelength trend can serve as *a-priori* constraints for  
230 reconstructing the course and geometry of the bedrock outlining the overdeepening.

231

#### 232 3.2 Assessing the gravity signal of the Quaternary sediments overlying the overdeepening

233 Subtracting the Bouguer anomalies values measured along a profile from the regional gravity field along  
234 the same profile yields what is referred to as the residual gravity anomaly. The related values provide  
235 information about a near-surface body or structure with a bulk density different from that of the  
236 surrounding bedrock (Kissling and Schwendener, 1990). Bandou et al. (2022; 2023) used this concept  
237 to determine the gravity signal of the Quaternary sediments overlying the Molasse bedrock. They

238 proceeded by calculating the residual gravity anomaly values along 10 profiles perpendicular to the  
239 inferred course of the Aare main overdeepening (black lines in Figure 2c). Note that because the  
240 Quaternary deposits have a lower bulk density than the Molasse bedrock, the occurrence of such  
241 deposits results in a negative residual gravity anomaly (Kissling and Schwendener, 1990). Accordingly,  
242 a larger bulk mass of Quaternary sediments yields a stronger (and thus a more negative residual  
243 anomaly) signal than a fill with less Quaternary material (Kissling and Schwendener, 1990; Bandou et  
244 al., 2022). Following this concept, we compiled the residual anomaly data from Bandou et al. (2023)  
245 for each gravity profile and drafted a contour map where each line displays the same residual anomaly  
246 value. This map was drawn by hand, thereby considering the *a-priori* information about the orientation  
247 of the Aare main overdeepening (Reber and Schlunegger, 2016).

248

### 249 3.3 *Estimating the thickness of Quaternary sediments based on gravity data*

250 Residual gravity anomaly values can be converted to thicknesses of Quaternary sediments through  
251 modelling, provided that *a-priori* data is available (Kissling and Schwendener, 1990). This includes  
252 information on: (i) density contrasts between the Molasse bedrock and the Quaternary fill, (ii) depths  
253 of bedrock encountered in drillings, and (iii) an already existing bedrock topography model (in our case  
254 the bedrock topography model of Reber and Schlunegger, 2016). Bandou et al. (2023) used a 3D gravity  
255 software referred to as PRISMA (Bandou, 2023b) to implement this approach, modelling the residual  
256 gravity anomalies along six profiles (Figure 5b) where the aforementioned *a-priori* data is well  
257 constrained. Note that upon using PRISMA, the geometry of the overdeepening fill was approximated  
258 by Bandou et al. (1922, 1923) through multiple right-handed prisms oriented as perpendicularly as  
259 possible to the profile of interest (Nagy, 1966; Banerjee and Das Gupta, 1977). We compiled the results  
260 of the PRISMA modelling presented by Bandou et al. (2022, 2023) to draw a map displaying the  
261 thickness distribution of Quaternary sediments overlying the Aare main overdeepening. When creating  
262 this map, we considered that a trend towards smaller or larger negative residual anomalies indicates a  
263 thinning or thickening of the Quaternary sediments, respectively (Kissling and Schwendener, 1990;  
264 Bandou et al., 2023). The difference between the elevation of the modern topography and the thickness  
265 of the Quaternary sediments returns a map displaying the bedrock topography.

266

### 267 3.4 *Combining the results of the gravity survey with drilling data to reconstruct the details of the* 268 *bedrock topography*

269 We updated the bedrock model of Reber and Schlunegger (2016) with information about the general  
270 shape of the overdeepening retrieved through gravity modelling outlined above, and we additionally  
271 considered the information of >100 drillings that were sunk >50 m deeply into the subsurface during  
272 the past years. Similar to Reber and Schlunegger (2016), we manually drew the isohypses of the  
273 bedrock, inferring that changes in the orientation of the contour lines and the depths of the bedrock were

274 gradual. We finally combined the map displaying the geometry of the bedrock beneath the  
 275 overdeepening with the elevation data provided by the 2 m-SwissAlti3D DEM (based on LIDAR data  
 276 of swisstopo) to present the shape of the bedrock topography as shaded relief.

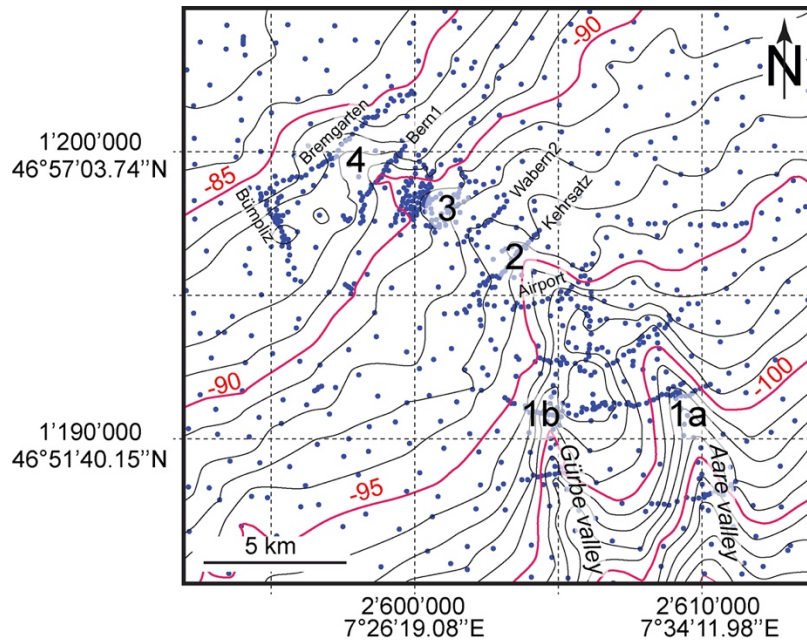


Figure 4

277  
 Figure 4: Bouguer anomalies, calculated with the density of the Molasse bedrock ( $2500 \text{ kg/m}^3$ ). The blue dots are gravity data taken from the Gravimetric Atlas of Switzerland (Olivier et al., 2008; 2011; swisstopo) and from Bandou (2023a). The isogals, indicated in mGal, illustrate the general gravity trend in the region and deviations thereof. 1a and 1b are sites located in the Aare and Gürbe valleys, respectively. These are the locations where the isogals have the largest deflections from the large-wavelength trend. Farther to the N (site 2) and then to the NW, the deflections decrease, reaching the lowest values at site 3. They increase again towards site 4 and then fade towards the NW. The figure also shows the locations of the gravity profiles presented in Bandou (2022) and Bandou et al. (2023). The grid corresponds to the Swiss coordinate system (CH1903+). Longitudes and latitudes are also indicated.

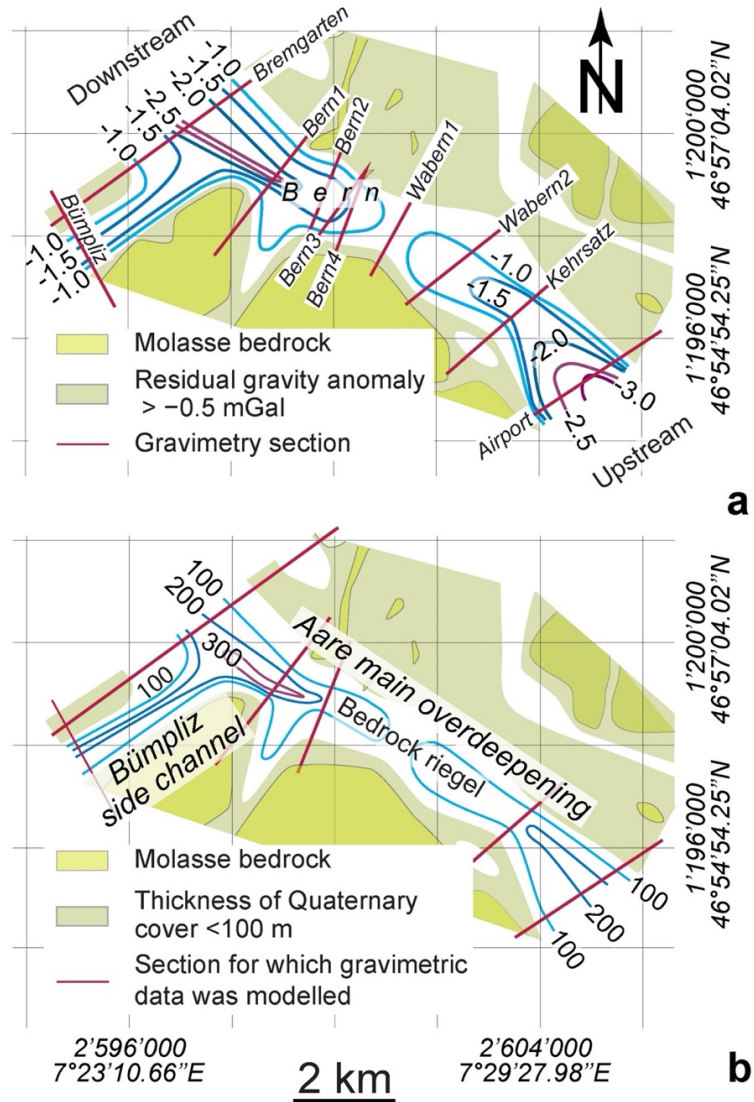
278

## 279 4 Results

### 280 4.1 Isogals and gravity signal of the bedrock topography beneath the overdeepening

281 The isogals calculated with the density of bedrock ( $2500 \text{ kg/m}^3$ ) clearly depict the general gravity trend,  
 282 which is characterized by a continuous SE-directed increase of the Bouguer anomaly values from -85  
 283 mGal in the NW to -105 mGal towards the SE (Figure 4). Note that a more negative value implies a  
 284 stronger gravity anomaly. The isogals generally strike SW-NE, reflecting the orientation of European  
 285 continental lithosphere, which gently dips beneath the Alpine orogen. However, and most importantly  
 286 in our context, the isogals also deviate from this pattern by being deflected towards the NW, where we  
 287 expect the occurrence of the Gürbe tributary trough and the Aare main overdeepening. This anomaly  
 288 (or deflection) has indeed the largest amplitudes of  $>4 \text{ mGal}$  and  $>3 \text{ mGal}$  beneath the Aare (location  
 289 1a on Figure 4) and Gürbe valleys, respectively (location 1b). This indicates that the depth of the  
 290 overdeepened trough is greatest there. Farther to the NW, the amplitude of the deflection decreases from  
 291 approximately  $3 \text{ mGal}$  at site 2 (between Airport and Kehrstatz) to  $<1 \text{ mGal}$  at site 3 (Figure 4),

292 suggesting a shallowing of the bedrock trough and thus the occurrence of a swell (or riegel). From there,  
 293 the amplitude increases again at site 4 as the trough appears to deepen once more, after which the  
 294 anomaly fades farther to the NW.  
 295



296

Figure 5

Figure 5: Residual gravity anomalies, representing the gravity signal of Quaternary sediments, and inferred thicknesses of Quaternary deposits. a) The contour lines of the residual gravity signals (mGal) caused by the Quaternary fill of the Aare main overdeepening are mainly based on gravity surveys along 10 sections (red lines; Bandou et al., 2023). Here, more negative values imply a greater signal caused by the bulk mass of Quaternary sediments overlying the overdeepened trough (Kissling and Schwendener, 1990; Bandou et al., 2022). b) Spatial distribution of Quaternary sediments, here expressed by the related thicknesses. These are mainly based on the results of gravity modelling, where Quaternary mass and its spatial distribution was forward modelled until a best-fit between the modelled and observed gravity signals of the Quaternary mass overlying the overdeepened trough was reached (Bandou, 2023; Bandou et al., 2023). Note that only the residual gravity anomalies of the Airport, Kehrsatz, Bern2, Bern1, Bremgarten and Bümpliz sections were modelled by Bandou et al. (2023). The grid refers to the Swiss coordinate system (CH1903+). Longitudes and latitudes are also indicated.

297

298 4.2 *Gravity signals of the Quaternary sediments overlying the overdeepening*

299 The residual gravity anomalies, which correspond to the gravity signal of the Quaternary sediments,  
300 reveal the same pattern as the isogals where the Bouguer anomaly values were calculated with the  
301 bedrock density of 2500 kg/m<sup>3</sup>. For the section across the Gürbe and Aare valleys (Figure 2c), Bandou  
302 et al. (2022; 2023) showed that the Quaternary fill of the Aare main overdeepening results in a gravity  
303 signal that ranges between c. -4.0 and -0.5 mGal. In addition, they showed that this signal changes from  
304 upstream to downstream: In particular, along the Gürbe-Aare transect (Figure 2c), which also crosses  
305 the Belpberg mountain ridge made up of Molasse bedrock, the strength of the signal ranges from c. -  
306 2.9 mGal in the Gürbe valley to c. -4.1 mGal in the Aare valley (Bandou et al., 2022). Farther  
307 downstream, the residual anomaly values and thus the signal of the overdeepening fill decreases, where  
308 the corresponding values change from c. -3.0 mGal (Airport profile) to approximately -1.5 and finally  
309 c. -1.0 mGal along the Kehrsatz and Wabern2 profiles, respectively (Figure 5a). The weakest signals  
310 with values between c. -0.5 mGal and -1 mGal were reported for the Wabern1 profile (Bandou et al.,  
311 2023; Figure 5a). This suggests a decrease in the mass of Quaternary sediments approaching Wabern1,  
312 most likely due a shallowing of the bedrock forming a riegel in this area. Farther downstream, the  
313 gravity signal of the Quaternary fill increases again and reaches values between c. -1.0 and c. -2.0 mGal  
314 along the Bern sections, and then approximately -2.5 mGal along the Bremgarten section c. 2 km farther  
315 downstream. This points towards an increase in the Quaternary mass and thus towards a deepening of  
316 the trough in this direction. The residual anomaly data thus clearly depict the course of the Aare main  
317 overdeepening, which strikes SE-NW in the city area of Bern (Figures 2c, 5a). Towards the NW margin  
318 of the study area, a second overdeepening referred to as the Bümpliz tributary trough (Schwenk et al.,  
319 2022a) strikes SW-NE and converges with the Aare main overdeepening NW of Bern. The gravity  
320 signal of the Bümpliz sedimentary fill is less and reaches a value of c. -1.5 mGal (Figure 5a; Bandou et  
321 al., 2023). Finally, the upstream side of the inferred bedrock riegel dips gentler than the downstream  
322 side, which is twice as steep: on the stoss side, the residual gravity anomalies change from <-2.5 mGal  
323 to >-1.0 mGal over a downstream distance of c. 4 km whereas on the lee side, the same change in the  
324 gravity signal occurs over only 2 km. Given that the residual gravity signal is a direct response of the  
325 bulk mass of Quaternary sediments overlying the Molasse bedrock (see section 4.2), and thus their  
326 volume supposing a lower density than the Molasse bedrock (see next section and Bandou et al., 2022;  
327 2023), the differences in the upstream and downstream gradients of the residual gravity anomaly values  
328 disclose the contrasts in the dip angles of the bedrock topography.

329

330 4.2 *Thickness of Quaternary sediments*

331 Available drilling information shows that the Quaternary fill in the Bern region generally consists of an  
332 alternation of gravel, sand and mud (Figure 2d), which have a bulk density that ranges from 2150 kg/m<sup>3</sup>  
333 for material at the base of the overdeepening fill, to 2000 kg/m<sup>3</sup> for the sediments towards the top. Based

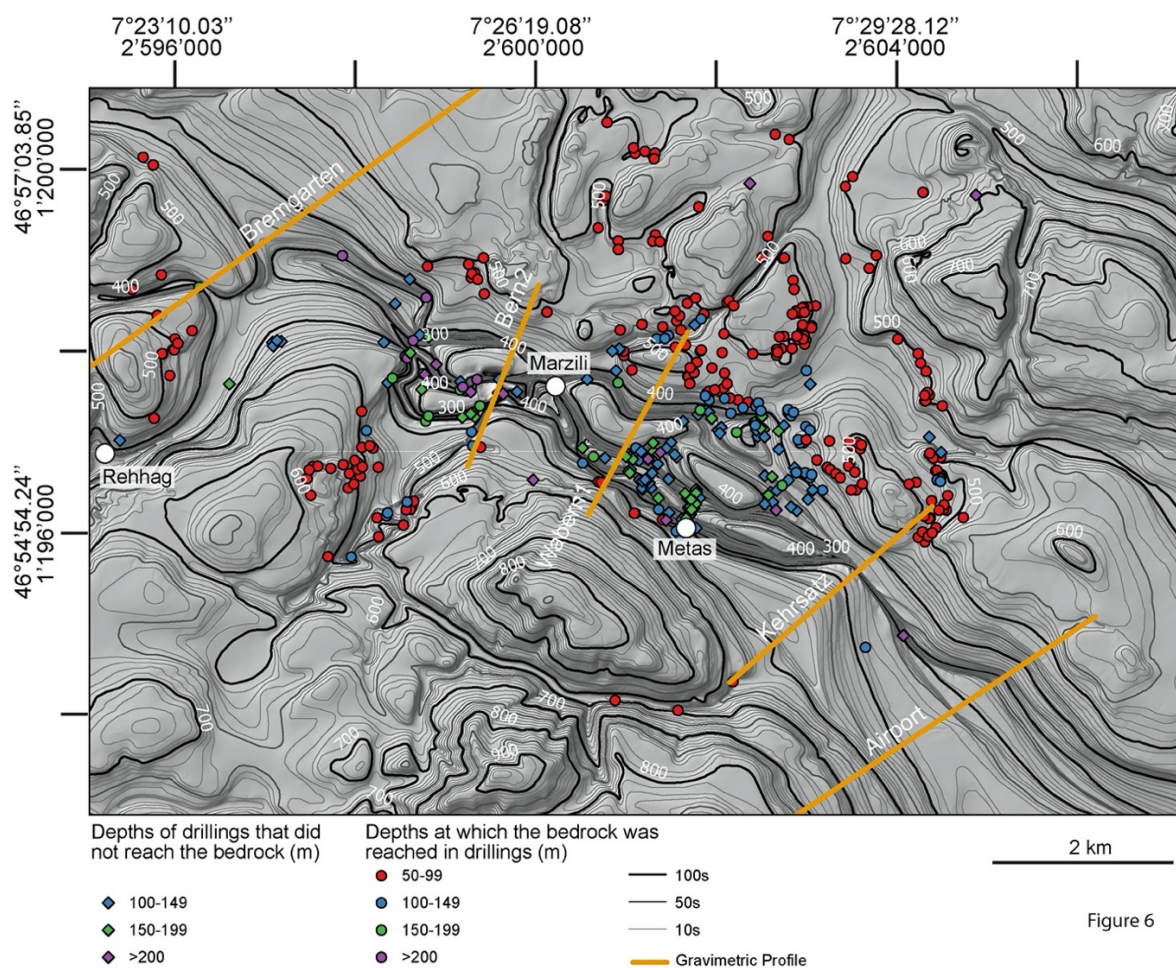
334 on a sensitivity analysis where the gravity response to different densities for the Quaternary sediments  
335 was evaluated, Bandou (2023a) and Bandou et al. (2022, 2023) could exclude the possibility that the  
336 Bouguer anomaly and residual anomaly patterns displayed in Figures 4 and 5a could be explained by  
337 spatial differences in the sedimentary architecture of the Quaternary fill. For instance, the low residual  
338 gravity anomalies displayed in the region of the Wabern2 profile (Figure 5a) would require an  
339 amalgamation of highly compacted glacial till. However, this is not consistent with the stratigraphic log  
340 of the core drilled at Metas (Figure 2d), which is made up of an alternation of sand, mud and gravel that  
341 was most likely deposited in a lacustrine environment. Instead, we prefer a perspective where the pattern  
342 of residual gravity anomaly values reflects spatial variations in the thickness of the Quaternary  
343 sediments. Accordingly, the thickest Quaternary suite can be found upstream and downstream of Bern  
344 (Figure 5b), where the Aare main overdeepening is between 4 and 5 km wide and >200 m deep,  
345 consistent with drilling information (Bandou et al., 2023). In the city area of Bern, however, the main  
346 trough tends to become shallower. This is indicated by the thickness of the Quaternary sediments  
347 reaching 100 m and possibly less (Figure 5b). The thickness of the Quaternary sediments filling the  
348 trough then increases again farther downstream.

349

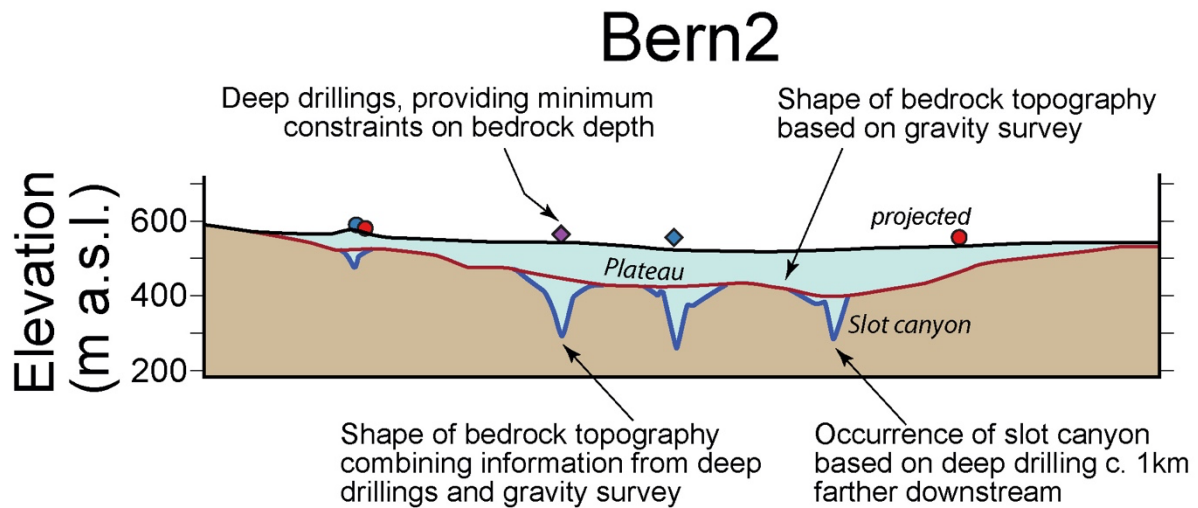
#### 350 *4.3 The consideration of deep drillings discloses the occurrence of slot canyons*

351 The reconstructed bedrock topography of the target region reveals a complex pattern (Figure 6), which  
352 can be described as a bedrock riegel that is dissected by multiple, partly anastomosing slot canyons or  
353 inner gorges (Bandou et al., 2023). At this stage, we cannot precisely reconstruct the number of the  
354 inferred canyons because we lack a high-resolution database of deep drillings (Figure 6). Yet, the  
355 discrepancy between (i) a relatively low gravity signal particularly between the Wabern2 and the Bern  
356 sections (Figure 5a) and (ii) drillings that reached the bedrock at much deeper levels >200 m below the  
357 surface (Figures 6) can only be resolved by invoking the occurrence of a plateau at shallow elevations  
358 that is dissected by one or multiple slot canyons (Figure 7). These gorges are up to 150 m deep and may  
359 connect the overdeepened basins upstream and downstream of the city area of Bern. In particular, south  
360 of Bern along the Aare profile (Figures 2b and 8a), the Aare main overdeepening has a cross-section  
361 that displays two superimposed levels of U-shapes, each of which with steep lateral flanks and a flat  
362 base. While the upper flat base occurs at an elevation of c. 450 m a.s.l., the lower flat contact to the  
363 bedrock is situated at c. 250 m a.s.l. and thus approximately 200 m deeper than the upper level (Bandou  
364 et al., 2022). Approximately 5 km farther downstream along the Airport section (Figures 2b, 8b), the  
365 cross-sectional geometry of the Aare main overdeepening maintains its generally U-shaped geometry  
366 with a base at an elevation between 200 and 250 m a.s.l. There, the base of the overdeepening appears  
367 less flat than farther upstream, but we acknowledge that the density of deep drillings in the region  
368 (Figure 6) and the resolution of the gravity data (Figure 5a, Bandou et al., 2023) is not high enough to  
369 fully support this comparison. Upon approaching the city area of Bern, the base of the bedrock becomes

370 shallower and appears to evolve towards a plateau particularly between the Kehrsatz and Bern2 sections  
 371 (Figures 6, 7, 8c, d and e). This plateau is situated at an elevation of c. 400 m a.s.l. (dashed lines on  
 372 Figure 8) and dissected by multiple slot-canyons, as evidenced by drillings reaching depths down to c.  
 373 300 m a.s.l. and even lower elevations, yet the canyons remain undetected by the gravity survey. This  
 374 implies that the canyons must be cutting up to 150 m deep below the plateau at c. 400 m a.s.l. and that  
 375 they are too narrow to be detected by the gravity survey (Bandou al., 2023). Farther to the Northwest  
 376 reaching the terminal part of the Aare main overdeepening (Figure 2b), the trough widens again and  
 377 gives way to a relatively deep basin where the deepest part occurs at an elevation of almost 300 m a.s.l.  
 378 (Figures 6, 8f). This terminal basin appears to be connected with the Bümpliz tributary trough farther  
 379 to the SW. Yet the density of drillings is too low (Figure 6) to determine whether a possible bedrock  
 380 swell separates the Aare main overdeepening from the Bümpliz tributary trough (Figure 2b).



381 Figure 6: Hillshade DEM, illustrating the bedrock topography of the Bern area, together with deep drillings  
 382 that either reached the bedrock (circles) or that ended in Quaternary sediments (diamonds). The shallow  
 drillings (<50 m) are not displayed on this map since the number is too large (more than 1000, please see  
 Reber and Schlunegger, 2016). The isohypses were drawn for every 10 m. The coordinates along the figure  
 margin refer to the Swiss coordinate system (CH1903+). The sections shown on this map are used to illustrate  
 the cross-sectional geometry of the overdeepening beneath Bern (see next figures).



383

Figure 7

Figure 7: Example that illustrates how we proceeded upon reconstructing the bedrock topography beneath Bern. We started with the general shape of the bedrock topography using the gravity signal of the bulk Quaternary mass as a basis (red line, and Figure 5b). Information from drillings >50 m deep (circles and diamonds: see Figure 6 for explanation of colors) allowed then to reconstruct the course and geometry of the slot canyons (blue line). The mass of their Quaternary fill is too low to be identified by the gravity survey. This is the case because the strength of a gravity signal decays exponentially with depth (see also Bandou et al., 2023, for further explanations).

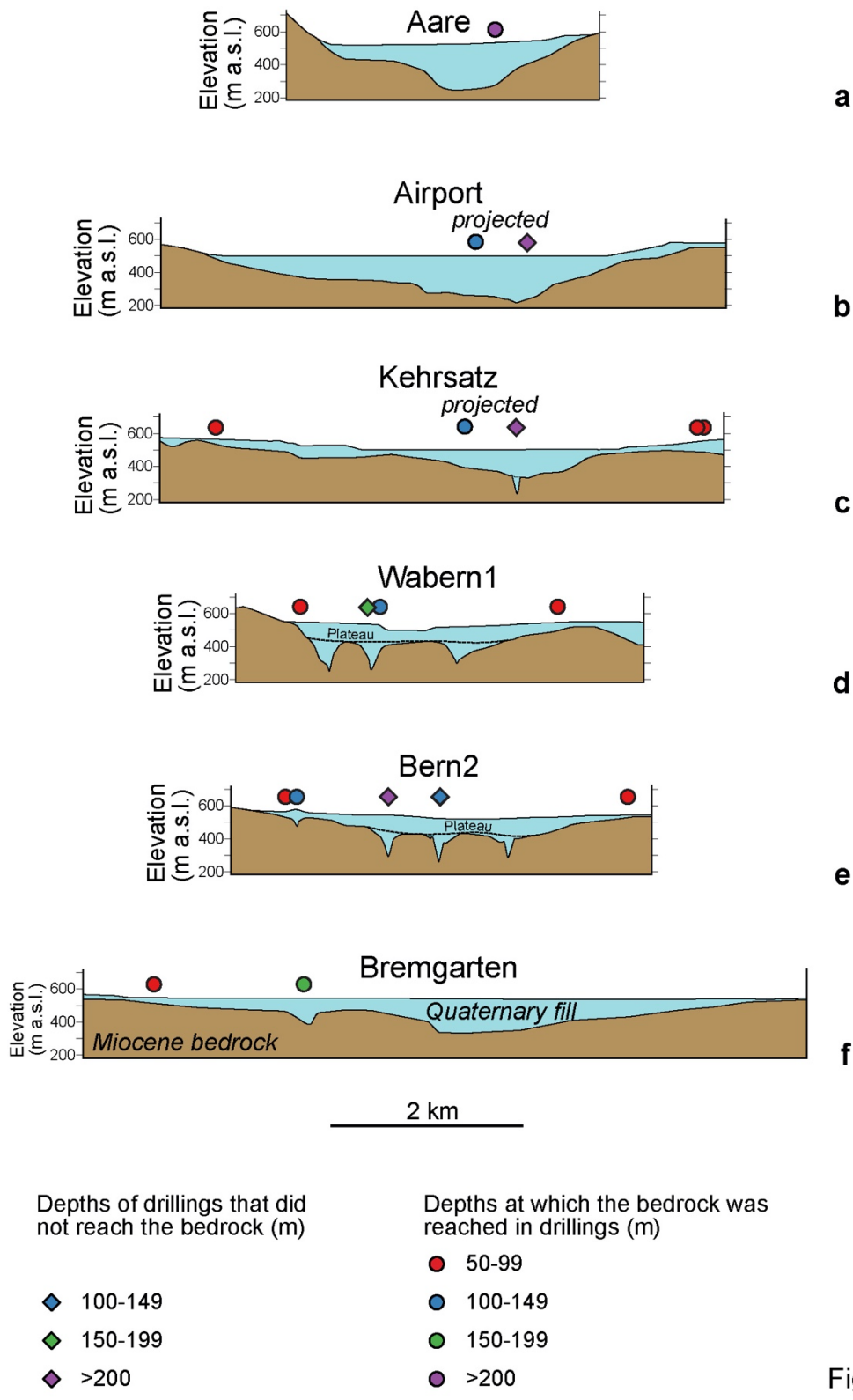
384

## 385 5 Discussion

### 386 5.1 Limitations upon reconstructing the bedrock topography model

387 The inferred existence of a bedrock riegel and slot canyons below Bern is based on two features: (i)  
 388 gravimetric data showing a relatively low negative anomaly, which we interpret as a relatively low  
 389 depth to bedrock in the Bern city area, and (ii) previous borehole logs that show a much greater drilled  
 390 depth to bedrock. Indeed, the combination of deep bedrock detected from borehole data in an area of  
 391 otherwise characterized by shallow bedrock, as imaged by gravimetry, suggests that the canyons must  
 392 extend deeply while remaining highly confined in order to stay below the spatial resolution of the  
 393 gravimetry method. However, we acknowledge that no direct drilling evidence confirms the presence  
 394 of such a riegel. Nevertheless, the contour lines of the Bouguer anomaly values, calculated using a  
 395 density of bedrock ( $2500 \text{ kg/m}^3$ ), indicate that the target overdeepening is generally broad and deep  
 396 upstream of Bern, shallow beneath the city, and then narrows and deepens downstream of it (Figure 4).  
 397 In addition, gravity data collected at 10 gravity stations along the Bern2 profile does point towards the  
 398 occurrence of a residual anomaly signal with a short wavelength beneath the main large-wavelength  
 399 residual gravity anomaly (Figures S1a and S1b in the Supplement). Indeed, using the results of 3D  
 400 gravity modelling, Bandou et al. (2023) considered the anomaly with the large wavelength as the gravity  
 401 response of the Quaternary fill overlying the bedrock riegel, whereas the short-wavelength anomaly  
 402 beneath it illustrates the possible occurrence of a slot canyon, filled by Quaternary sediments (Figure

403 S1c in the Supplement). Further slot canyons could not be identified upon modelling due to a lack of  
 404 resolution of the gravimetric data.



405 Figure 8: Sections through the Bern area, where the geometry of the bedrock is taken from the DEM  
 406 illustrated in Figure 6. The Aare section is taken from Bandou et al. (2022). See Figures 2 and 6  
 for location and orientation of sections.

407 In summary, we are confronted with the situation that there is most likely a bedrock riegel imaged by  
408 the gravity data, and that thick Quaternary deposits (deep erosion) have been encountered in some deep  
409 drillings as well (and have also been detected in the Bern2 gravity profile; Figures S1a to S1b in the  
410 Supplement). We thus propose an interpretation where a bedrock riegel is cut by narrow slot canyons  
411 filled with Quaternary sediments, as such a scenario adequately combines the findings from our gravity  
412 survey and drilling information. Furthermore, using the modern examples such as the Aare gorge  
413 displayed on Figure 3a as a basis, we interpret that these slot canyons formed the hydrological link  
414 between the upstream and downstream basins. We exclude an alternative interpretation where the drilled  
415 Quaternary sequences represent the filling of isolated glacial potholes. Indeed, the short distance  
416 between the individual boreholes with thick Quaternary sequences and the almost linear arrangement  
417 of these boreholes, particularly near Wabern1 (Figure 6), suggests that the drilled sequences comprise  
418 the fill of continuous channels rather than potholes.

419

## 420 5.2 *Subglacial origin and the role of subglacial meltwater*

421 It is agreed upon in the literature that the formation of overdeepened basins can be understood as the  
422 response of erosion by glaciers. The main arguments that have been put forward are (i) the depths of  
423 the base of these depressions, which are generally below the current fluvial base-level, and (ii) the  
424 occurrence of adverse slopes in the downstream direction of these basins (Figure 1, Preusser et al., 2010;  
425 Patton et al., 2016; Alley et al., 2019; Magrani et al., 2022; Gegg and Preusser, 2023). Such geometric  
426 features are also encountered for the Aare main overdeepening beneath the city area of Bern. Therefore,  
427 the origin of this depression has repeatedly been interpreted as the response of the erosional processes  
428 of a glacier with a source in the Central Alps of Switzerland (Dürst Stucki et al., 2010; Preusser et al.,  
429 2010; Reber and Schlunegger, 2016; Magrani et al., 2022; Bandou et al., 2023). As a refinement already  
430 outlined by Bandou et al. (2023) and further detailed in this work, the overdeepening beneath Bern can  
431 be subdivided into a southeastern and a northwestern sub-basin. These depressions are separated by a  
432 bedrock riegel or swell, which itself is dissected by one or multiple slot canyons establishing a  
433 hydrological link between the upstream and downstream basins (Figure 6). Such ensembles of basins,  
434 riegels and slot canyons (or inner gorges) are common features in Alpine valleys (Figure 3) and have  
435 therefore been the target of previous research. In this context, it was proposed that such gorges and  
436 riegels in the Alps were likely shaped during several glacial/interglacial periods (Montgomery and  
437 Korup, 2011), and that the incision of the canyons occurred during the decay of glaciers and ice caps,  
438 when large volumes of meltwater were released (Steinemann et al., 2021). As further, yet only partly  
439 related examples, erosion by subglacial meltwater was put forward to explain the formation of inner  
440 gorges at the margin of the Fennoscandian ice sheet (based on the pattern of surface exposure ages;  
441 Jansen et al., 2014), and such a mechanism was used to explain (i) the origin of the deep channels on  
442 the floor of the eastern English Channel, and (ii) the breaching of the bedrock swell at the Dover strait  
443 during the aftermath of the Marine Isotope Stage (MIS) 12 or a later glaciation (Gupta et al., 2007;

444 Cohen et al., 2014; Gupta et al., 2017). In this context, Jansen et al. (2014) noted that typical field  
445 evidence for inferring a subglacial meltwater control includes (i) the occurrence of anastomosing  
446 channels, (ii) undulating valley long profiles, and (iii) a topography that apparently amplifies the  
447 hydraulic potential. The resolution of our data is not enough to see such details of the valley long  
448 profiles, but sufficient to display the anastomosing patterns of the slot canyons, with channels  
449 meandering, splitting and merging again (Figure 6).

450

### 451 5.3 *Formation through erosion by subglacial meltwater inferred from theory and modelling*

452 Besides the geometrical arguments and field-based observations outlined in the previous section, a  
453 subglacial meltwater influence on the formation of overdeepenings has also been inferred based on  
454 theoretical considerations, including the relationships between meltwater runoff and the sediment  
455 transport capacity of proglacial and subglacial streams (e.g., Boulton and Hindmarsh, 1987; Alley et  
456 al., 1997; Herman et al., 2011, Beaud et al., 2016). Because sediment transport increases exponentially  
457 with both the volume and seasonality of meltwater runoff, Alley et al. (1997) interpreted that subglacial  
458 and proglacial streams are among the most efficient sediment-transport mechanisms on Earth. This  
459 process peaks in the ablation zone of a glacier, where surface melt reaches the bed and significantly  
460 contributes to the generation of subglacial runoff. Also on theoretical grounds, Cohen et al. (2023)  
461 showed that subglacial meltwater is able to remove the sediment from the base of a glacier and to further  
462 incise into bedrock provided that the pressure of the subglacial meltwater and that of the ice overburden  
463 are at least the same (Boulton and Hindmarsh, 1987). The results from the model of Cohen et al. (2023),  
464 tailored to determine the location of the subglacial drainage pathways, further suggest that such  
465 conditions most likely prevailed at the front of piedmont glaciers and particularly during the decaying  
466 stage of a glacier when large volumes of meltwater were available. In addition, the model predicts that  
467 under such circumstances, the locations of subglacial meltwater pathways are likely to coincide with  
468 segments where high rates of glacial erosion occur (Cohen et al., 2023). Therefore, reaches with  
469 evidence for intense erosion by both water and ice occur in the same area and are hydrologically  
470 connected with each other. We propose this to be the case for the ensemble of overdeepened basins and  
471 slot canyons beneath Bern.

472

### 473 5.4 *The role of bedrock strength and the confluence of two glaciers*

474 The formation of riegels and basins is consensually understood as conditioned by differences in bedrock  
475 strengths. This also concerns the controls on the size of a basin itself where bedrock with a high  
476 erodibility tends to host a larger basin than lithologies where the erodibility is low (e.g., Magrani et al.,  
477 2020; Gegg and Preusser, 2023). Following this logic, swells preferentially would form in locations  
478 where the bedrock has a lower erodibility than the rock units farther upstream and downstream. This  
479 has been documented for the riegel in the Aare valley, which separates an overdeepened basin upstream

480 from a wide valley farther downstream (Figure 3a). There, the bedrock riegel is made up of the Quinten  
481 Formation (Gisler et al., 2020; Stäger et al., 2020). These limestones tend to have a lower erodibility  
482 (Kühni and Pfiffner, 2001) than the sandstone-marl alternations (North Helvetic Flysch; Gisler et al.,  
483 2020; Stäger et al., 2020) downstream of the bedrock swell, and the suite of sandstones, marls and  
484 dolomite beds upstream of it (Mels- and Quarten Formations; Gisler et al., 2020; Stäger et al., 2020).  
485 Another example is offered by the riegel in the Trift valley (Figure 3b), where the bedrock forming the  
486 ridge is made up of a banded, biotite-rich gneiss (Erstfeld gneiss). Upstream and downstream of the  
487 swell, the bedrock is cut by multiple faults and fractures, thus offering a lower resistance to erosion  
488 (Steinemann et al., 2021). In the Bern area, the bedrock architecture is comparable to the examples  
489 explained above where the UMM, which has a low erodibility, forms the swell, whereas the LFM with  
490 a relatively large erodibility constitutes the bedrock downstream of the riegel (section 2.3). In addition,  
491 the NW-SE striking faults in the Molasse bedrock (Isenschmid, 2019), which offer zones of mechanical  
492 weaknesses, most likely controlled the course of the slot canyons as they have the same orientation.  
493 Presumably as important as the contrasts in bedrock erodibility: the bedrock swell underneath Bern is  
494 situated in the confluence area between the Valais and Aare glaciers (Figure 2b). The occurrence of  
495 swells at the confluence areas is consistent with observations in Alpine valleys (Figure 3) and with  
496 topographic and bathymetric DEMs of overdeepenings in Labrador, Canada (Lloyd et al., 2023). In this  
497 case, the deep carving into the bedrock would be the result of an acceleration of the ice flow (Herman  
498 et al., 2015) in response to the increase in the ice flux downstream of the confluence region.  
499 Alternatively, a bedrock riegel could also form upstream of the confluence of two glaciers (see e.g., the  
500 Maggia valley as modern example, Figure 3c). For the Bern area, the damming of the Aare glacier by  
501 the much larger Valais glacier could have caused a reduction of the flow velocity of the Aare glacier  
502 (Figure 2b). Consequently, the shear velocity and thus the bedrock abrasion rates would decrease,  
503 thereby facilitating the preservation of a bedrock swell.

504

##### 505 *5.5 Differences in the geometries between the exposed riegels and basins in Alpine valleys, and the* 506 *overdeepening beneath Bern*

507 Despite obvious similarities between the geometric properties of the overdeepening system beneath  
508 Bern and the currently exposed riegels and slot canyons in Alpine valleys, there are also major  
509 differences (Figure 3 versus Figures 6 and 8). The most striking one is the occurrence, beneath Bern, of  
510 the riegel and inner gorges approximately 50-100 m below the current base-level, and the absence of  
511 an obvious continuation of the thalweg NW of Bern (Figure 2c). Accordingly, the inferred interpretation  
512 where the slot canyons beneath Bern were formed by subglacial meltwater requires a mechanism where  
513 the meltwater is not only capable to incise into bedrock beneath a glacier, but also to escape the  
514 depression by ascending nearly 200 m from the base of the overdeepening to the surface near the  
515 glacier's snout. Using Bernoulli's principle as a basis (e.g., Batchelor, 1967), it was proposed that such

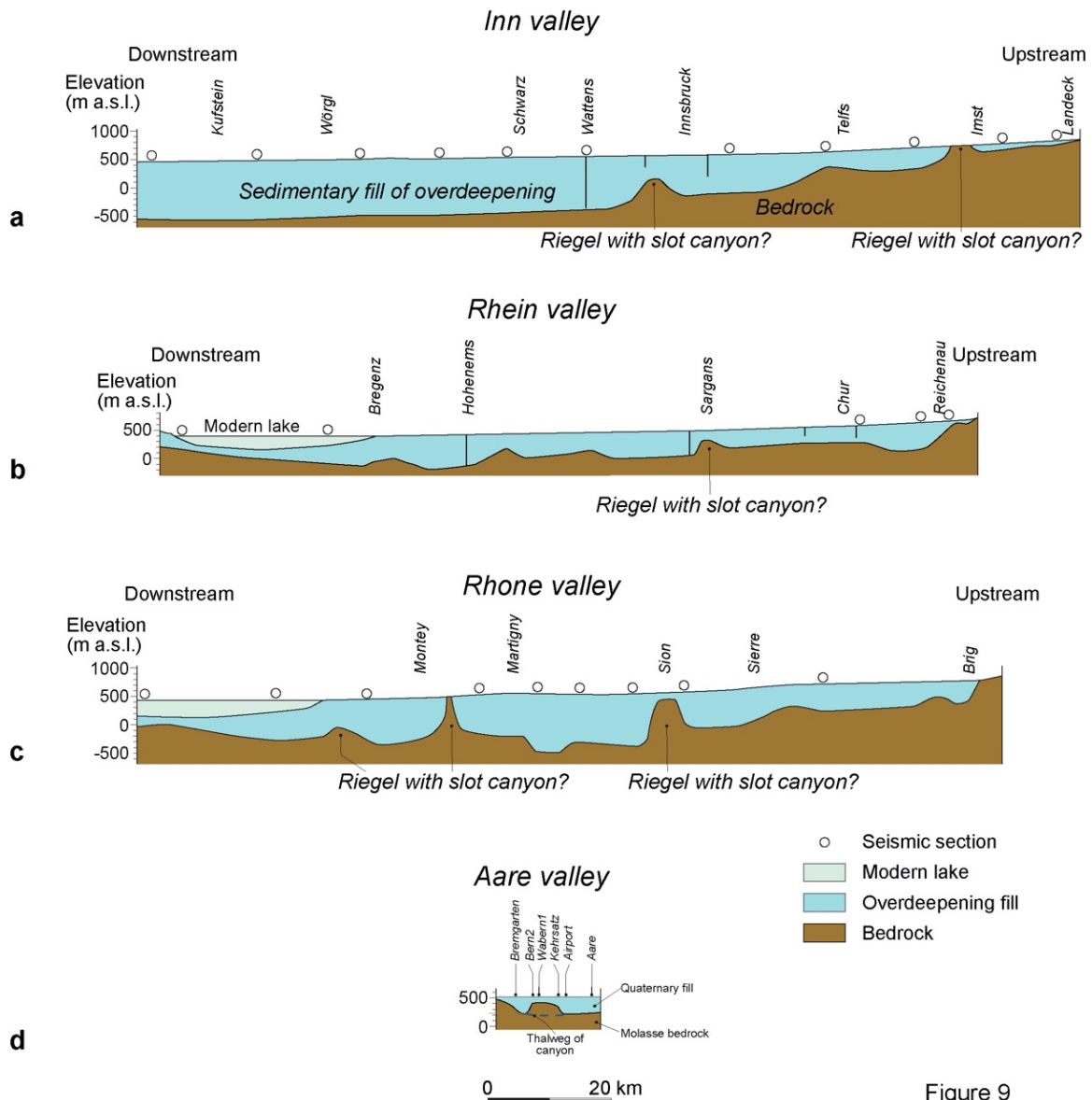
516 an ascent of subglacial meltwater was driven by the translation of high hydrostatic pressure into  
517 hydrodynamic pressures at the downstream margin of a glacier (Dürst Stucki and Schlunegger, 2013).  
518 Such a mechanism is most effective at work where the surface slope of a glacier is steeper than the  
519 adverse slope of an overdeepening (Hooke and Pohjola, 1994), as is commonly found in the frontal part  
520 of a glacier (Figure 1a). Since the ratio between the densities of ice and water is  $>0.9$  (Harvey, 2019),  
521 the inferred 200 m-rise of the meltwater requires a minimum hydrostatic pressure corresponding to  
522  $>220$  m-thick ice to allow an upward water flow. Such a scenario is plausible, as the Aare glacier in the  
523 Bern area was estimated to have reached several hundred meters in thickness during past glaciations  
524 (Bini et al., 2009; Preusser et al., 2011; Figure 2b). If this hypothesis is valid, then the thickness of the  
525 piedmont glaciers sets an uppermost limit to the depth at which overdeepenings can be carved into the  
526 bedrock, since it represents the driver of overpressure required for the subglacial meltwater to ascend  
527 to the surface from deeper levels.

528

## 529 **6 Conclusions**

530 Bedrock riegels separating upstream and downstream basins are common features in modern Alpine  
531 valleys, and they have been documented from overdeepenings in the region of Bern. We propose that  
532 these riegels occur as ensembles together with slot canyons that cut through these swells and establish  
533 a hydrological link between the upstream and downstream basins. We suggest this based on our  
534 reconstruction of the bedrock topography of the Aare main overdeepening in the Bern area, and we  
535 propose that such ensembles of basins, riegels and slot canyons also occur in other Alpine  
536 overdeepenings such as the Rhone, Rhine and Inn valleys (Figure 9). We further suggest that these slot  
537 canyons were formed through incision by glacial meltwater during the deglaciation when large volumes  
538 of meltwater were available. As the flow must counteract adverse slopes, it may also be envisioned that  
539 the slot canyons formed during glacial maxima, when ice thickness (and thus excess hydrostatic  
540 pressure) is maximum, driving vigorous underflows. For the bedrock swell underneath Bern, the  
541 resolution of the dataset presented in this work does not allow to locate and reconstruct the precise  
542 course of the inferred slot canyons. However, the presented reconstruction of the bedrock topography  
543 reconciles (i) the occurrence of low residual gravity anomalies in the Bern area (Figure 5a), which  
544 suggests a topographic high of the incised bedrock marking the base of the overdeepening, and (ii) the  
545 significant depth at which Quaternary sediments were encountered in drillings, indicating deep-reaching  
546 bedrock incision (Figures 6, 7). In many Alpine valleys, such ensembles of riegel and slot canyons  
547 appear to be preferentially formed in the confluence area between two glacial valleys and where the  
548 bedrock has a relatively low erodibility. We posit that this configuration is also valid for the  
549 overdeepening below the Bern area, where such a bedrock swell appears to be situated just upstream of  
550 the confluence between the Aare and Valais glaciers, at least during LGM times and possibly during

551 previous glaciations. In addition, the inferred bedrock riegel beneath Bern is located where the bedrock  
 552 has a lower erodibility than farther downstream.



553 Figure 9

Figure 9: Sections showing the patterns of overdeepenings from upstream to downstream for a) the Inn valley, b) the Rhine valley, c) the Rhone valley and d) the Aare valley in the Bern area. The examples of the Inn, the Rhine and the Rhone valleys are taken from Hinderer (2001), whereas the section along the Aare valley is a modified version of Bandou et al. (2023) and bases on the data presented in Figure 6. The data from the Aare valley covers a short distance only, but it shows a striking similarity to the riegels in the large Alpine valleys. Therefore, it is quite likely that the other riegels are also dissected by narrow channels and that all settings share a similar origin.

554  
 555 In summary, we present a bedrock model that documents an upstream-downstream trend of the  
 556 subglacial drainage network: (i) Along the Aare cross-section, which is situated upstream of the riegel  
 557 there appears to be no evidence of a channelised subglacial drainage network incising into the bedrock;  
 558 (ii) in the area of the inferred riegel, we postulate the occurrence of an anastomosing network of slot  
 559 canyons based on drilling information, which evolves (iii) downstream of the riegel into a single canyon  
 560 as seen along the Bremgarten cross-profile. This rises further questions about the mechanisms that could

561 be responsible for these changes in the network, how such processes evolved in space and time, and  
562 how possible variations in the subglacial drainage network would have affected bedrock erosion and  
563 ice flow. Answers to such following up questions require detailed constraints on the ages and the  
564 sedimentary architecture of the Quaternary fill, which are not available. Yet, the few chronological  
565 information published on the Quaternary fill of overdeepenings in the Swiss Plateau does support an  
566 interpretation where the deep carving occurred during multiple stages since the Middle Pleistocene  
567 Transition c. 800 ka ago (Schluchter, 2004). Apparently, the change in the frequency of glacial-  
568 interglacial cycles from a 40 ka- to a 100 ka-periodicity, which occurred at that time, not only resulted  
569 in rapid glacial erosion (Pedersen and Egholm, 2013) and in the deep glacial carving of U-shaped  
570 valleys in the Alps (Häuselmann et al., 2007, Valla et al., 2011), but also in the formation of  
571 overdeepenings with complex geometries including basins, riegels and slot canyons in the foreland.

572

573

#### 574 **Acknowledgement**

575 This work was financially supported by the Swiss National Science Foundation (project No.  
576 200021\_175555) with contributions from the Stiftung Landschaft und Kies, swisstopo and the  
577 Gebäudeversicherung Bern GVB.

578

#### 579 **Data availability**

580 All data used in this paper can be ordered by the Authorities of the Canton Bern and by the authors on  
581 request.

582

#### 583 **Author contributions**

584 EK designed the study, together with FS and DB. DB collected the gravity data and processed them,  
585 with support by UM and EK. FS wrote the paper and conducted the analyses and interpretation of the  
586 data. RR drafted the bedrock topography map. PS, MS, DM and GD contributed to the discussion. All  
587 authors approved the article.

588

#### 589 **Competing interests**

590 The authors declare that they have no conflict of interest.

591

#### 592 **References**

593 Alley, R.B., Cuffey, K.M., Evenson, E.B., Strasser, J.C., Lawson, D.E., and Larson, G.J.: How glaciers  
594 entrain and transport basal sediment: physical constraints. *Quat. Sci. Rev.*, 16, 1017-1038, 1997.  
595 Alley, R., Cuffey, K., and Zoet, L.: Glacial erosion: Status and outlook. *Ann. Glaciol.*, 60, 1–13,  
596 <https://doi.org/10.1017/aog.2019.38>, 2019.

597 Anderson, R.S., Molnar, P., and Kessler, M.A.: Features of glacial valley profiles simply explained. *J.*  
598 *Geophys. Res., Earth Surface*, 111, F01004, doi:10.1029/2005JF000344, 2006.

599 Anselmetti, F., Bavec, M., Crouzet, C., Fiebig, M., Gabriel, G., Preusser, F., Ravazzi, C., and Dove  
600 team.: Drilling Overdeepened Alpine Valleys (ICDP-DOVE): quantifying the age, extent, and  
601 environmental impact of Alpine glaciations. *Sci. Drill.*, 31, 51–70, [https://doi.org/10.5194/sd-](https://doi.org/10.5194/sd-31-51-2022)  
602 [31-51-2022](https://doi.org/10.5194/sd-31-51-2022), 2022.

603 Bandou, D.: Overdeepenings in the Bern region, Switzerland: Understanding their formation processes  
604 using 3D gravity forward modelling. PhD thesis, univ. Bern, Switzerland, 381pp,  
605 <https://boristheses.unibe.ch/id/eprint/4573>, 2023a.

606 Bandou, D.: Gravi3D: A 3D forward modelling software using gravity data to resolve the geometry of  
607 subsurface objects, <https://zenodo.org/doi/10.5281/zenodo.8153258>, 2023b.

608 Bandou, D., Schlunegger, F., Kissling, E., Marti, U., Schwenk, M., Schläfli, P., Douillet, G., and Mair,  
609 D.: Three-dimensional gravity modelling of a Quaternary overdeepening fill in the Bern area of  
610 Switzerland discloses two stages of glacial carving. *Scientific Rep.*, 12, 1441,  
611 <https://doi.org/10.1038/s41598-022-04830-x>, 2022.

612 Bandou, D., Schlunegger, F., Kissling, E., Marti, U., Reber, R., and Pfander J.: Overdeepenings in the  
613 Swiss plateau: U-shaped geometries underlain by inner gorges. *Swiss. J. Geosci.*, 116, 19,  
614 <https://doi.org/10.1186/s00015-023-00447-y>, 2023.

615 Banerjee, B., and Das Gupta, S.P.: Gravitational attraction of a rectangular parallelepiped. *Geophysics*,  
616 42, 1053–1055, 1977.

617 Batchelor, G. K.: An introduction to fluid dynamics (p. 615). Cambridge Univ. Press, 1967.

618 Beaud, F., Flowers, G.E., and Venditti, J.G.: Efficacy of bedrock erosion by subglacial water flow. *Earth*  
619 *Surf. Dyn.*, 4, 125-145, <https://doi.org/10.5194/esurf-4-125-2016>, 2016.

620 Bini, A., et al.: Die Schweiz während des letzteiszeitlichen Maximums (LGM) 1:500'000. Bundesamt  
621 für Landestopografie swisstopo, Bern, Switzerland, 2009.

622 Boulton, G.S., and Hindmarsh, R.C.A.: Sediment deformation beneath glaciers: rheology and  
623 geological consequences. *J. Geophys. Res.* 92, 9059-9082, 1987.

624 Brocklehurst, S.H., and Whipple, K.X.: Glacial erosion and relief production in the eastern Sierra  
625 Nevada, California. *Geomorphology* 42, 1–24, 2002.

626 Brocklehurst, S.H., Whipple, K.X., and Foster, D.: Ice thickness and topographic relief in glaciated  
627 landscapes of the western USA. *Geomorphology*, 97, 35-51,  
628 <https://doi.org/10.1016/j.geomorph.2007.02.037>, 2008.

629 Büchi, M. W., Frank, S. M., Graf, H. R., Menzies, J., and Anselmetti, F. S.: Subglacial emplacement of  
630 tills and meltwater deposits at the base of overdeepened bedrock troughs. *Sedimentology*, 64,  
631 685, <https://doi.org/10.1111/sed.12319>, 2017.

632 Büchi, M., Graf, H.R., Haldimann, P., Lowick, S.E. and Anselmetti, F.S.: Multiple Quaternary erosion  
633 and infill cycles in overdeepened basins of the northern Alpine foreland. *Swiss J. Geosci.*, 111,  
634 133-167, <https://doi.org/10.1007/s00015-017-0289-9>, 2018.

635 Burschil, T., Bunn, H., Tanner, D.C., Wiedlandt-Schuster, U., Ellwanger, D., and Gabriel, G.: High-  
636 resolution reflection seismics reveal the structure and the evolution of the Quaternary glacial  
637 Tannwald Basin. *Near Surf. Geophys.*, 16, 593-610, <https://doi.org/10.1002/nsg.12011>, 2018.

638 Burschil, T., Tanner, D., Reitner, J., Bunn, H., and Gabriel, G.: Unravelling the complex stratigraphy  
639 of an overdeepened valley with high-resolution reflection seismics: The Lienz Basin (Austria),  
640 *Swiss J. Geosci.*, 112, 341–355, <https://doi.org/10.1007/s00015-019-00339-0>, 2019.

641 Clark, P.U., and Walder, J.S. Subglacial drainage, eskers, and deforming beds beneath the Laurentide  
642 and Eurasian ice sheets. *Geol. Soc. Amer. Bull.*, 106, 304-314, [https://doi.org/10.1130/0016-7606\(1994\)106<0304:SDEADB>2.3.CO;2](https://doi.org/10.1130/0016-7606(1994)106<0304:SDEADB>2.3.CO;2), 1994.

644 Cohen, K. M., Gibbard, P. L., and Weerts, H. J. T.: North Sea palaeogeographical reconstructions for  
645 the last 1 Ma. *Neth. J. Geosci.* 93, 7–29, 2014.

646 Cohen, D., Juvet, G., Zwinger, T., Landgraf, A., and Fischer, U.H.: Subglacial hydrology from high-  
647 resolution ice-flow simulations of the Rhine Glacier during the Last Glacial Maximum: a proxy  
648 for glacial erosion. *E&G Quat. Sci. J.*, 72, 189-201, <https://doi.org/10.5194/egqsj-72-189-201>,  
649 2023.

650 Cook, S. J., and Swift, D. A.: Subglacial basins: Their origin and importance in glacial systems and  
651 landscapes. *Earth-Science Rev.*, 115, 332–372,  
652 <https://doi.org/10.1016/j.earscirev.2012.09.009>, 2012.

653 Dehnert, A., Lowick, S.E., Preusser, F., Anselmetti, F.S., Drescher-Schneider, R., Graf, H.R., Heller,  
654 F., Horstmeyer, H., Kemna, H.A., Nowaczyk, N.R., Züger, and Furrer, H.: Evolution of an  
655 overdeepened trough in the northern Alpine Foreland at Niederweningen, Switzerland. *Quat.*  
656 *Sci. Rev.*, 34, 127-145, <https://doi.org/10.1016/j.quascirev.2011.12.015>, 2012.

657 Dietrich, P., Griffis, N. P., Le Heron, D. P., Montañez, I. P., Kettler, C., Robin, C., and Guillocheau, F.:  
658 Fjord network in Namibia: A snapshot into the dynamics of the late Paleozoic glaciation.  
659 *Geology*, 49, 1521-1526, <https://doi.org/10.1130/G49067.1>, 2021.

660 Douillet, G., Ghienne, J. F., Géraud, Y., Abueladas, A., Diraison, M., and Al-Zoubi, A.: Late Ordovician  
661 tunnel valleys in southern Jordan. *Geol. Soc. London Spec. Publ.*, 368, 275-292,  
662 <https://doi.org/10.1144/sp368.4>, 2012.

663 Dürst Stucki, M., Reber, R., and Schlunegger, F.: Subglacial tunnel valleys in the Alpine foreland: An  
664 example from Bern, Switzerland. *Swiss J. Geosci.*, 103, 363–374,  
665 <https://doi.org/10.1007/s00015-010-0042-0>, 2010.

666 Dürst-Stucki, M., and Schlunegger, F.: Identification of erosional mechanisms during past glaciations  
667 based on a bedrock surface model of the central European Alps. *Earth Planet. Sci. Lett.*, 384,  
668 57–70. <https://doi.org/10.1016/j.epsl.2013.10.009>, 2013.

669 Egholm, D.L., Nielsen, S., Pedersen, V., and Lesemann, J.: Glacial effects limiting mountain height.  
670 *Nature*, 460, 884–887, <https://doi.org/10.1038/nature08264>, 2009.

671 Feiger, N., Huss, M., Leinss, S., Sold, L., and Farinotti, D.: The bedrock topography of Gries- and  
672 Findelengletscher. *Geogr. Helv.*, 73, 1–9, <https://doi.org/10.5194/gh-73-1-2018>, 2018.

673 Fischer, U., and Häberli, W.: Overdeepenings in glacial systems: Processes and uncertainties. *Eos*, 93,  
674 35, 341–341, <https://doi.org/10.1029/2012EO350010>, 2012.

675 Garefalakis, P., and Schlunegger, F.: Tectonic processes, variations in sediment flux, and eustatic sea  
676 level recorded by the 20 Myr old Burdigalian transgression in the Swiss Molasse basin. *Solid  
677 Earth*, 10, 2045–2972, <https://doi.org/10.5194/se-10.2045-2019>, 2019.

678 Gees: Spühlbohrung Bern B1. Wasser und Energiewirtschaft des Kantons Bern, 1974.

679 Gegg, L., Deplazes, G., Keller, L., Madritsch, H., Spillmann, T., Anselmetti, F. S., and Büchi, M.W.:  
680 3D morphology of a glacially overdeepened trough controlled by underlying bedrock geology.  
681 *Geomorphology*, 394, 107950, <https://doi.org/10.1016/j.geomorph.2021.107950>, 2021.

682 Gegg, L., and Preusser, F.: Comparison of overdeepened structures in formerly glaciated areas of the  
683 northern Alpine foreland and northern central Europa. *E&G Quat. Sci. J.*, 72, 23–36,  
684 <https://doi.org/10.5194/egqsj-72-23-2023>, 2023.

685 Geotest: Grundlagen für Schutz und Bewirtschaftung der Grundwasser des Kantons Bern.  
686 Hydrogeologie Gürbetal und Stockental. Wasser- und Energiewirtschaftsamt des Kantons Bern  
687 WEA, 123 pp, 1995.

688 Geotest: Kernbohrung Kb 97.1. Wasser und Energiewirtschaft des Kantons Bern, 1997.

689 Gerber, E.: Geologische Karte von Bern und Umgebung 1:25'000. Kümmerli und Frei, Bern, 1927.

690 Gisler, C., Labhart, T., Spillmann, P., Herwegh, M., Della Valla, G., Trüssel, M., and Wiederkehr, M.:  
691 Erläuterungen. Geologischer Atlas der Schweiz 1:25'000, 1210 Innertkirchen, Schweiz. *Geol.  
692 Komm.*, 2020.

693 Gupta, S., Collier, J.S., Palmer-Felgate, A., and Potter, G.: Catastrophic flooding origin of shelf valley  
694 systems in the English Channel. *Nature*, 448, 342–345, <https://doi.org/10.1038/nature06018>,  
695 2007.

696 Gupta, S., Collier, J. S., Garcia-Moreno, D., Oggioni, F., Trentesaux, A., Vanneste, K., De Batist, M.,  
697 Camelbeeck, T., Potter, G., Van Vliet-Lanoë, B., and Arthur, J. C. R.: Two-stage opening of  
698 the Dover Strait and the origin of island Britain. *Nat. Comm.*, 8, 15101,  
699 <https://doi.org/10.1038/ncomms15101>, 2017.

700 Häberli, W., Linsbauer, A., Cochachin, A., Salazar, C., and Fischer, U.H.: On the morphological  
701 characteristics of overdeepenings in high-mountain glacier beds. *Earth Surf. Proc. Landf.*, 41,  
702 1980–1990, <https://doi.org/10.1002/esp.396>, 2016.

703 Hantke, R., and Scheidegger, A. E.: Zur Genese der Aareschlucht (Berner Oberland, Schweiz). *Geogr.*  
704 *Helv.*, 48, 120–124, <https://doi.org/10.5194/gh-48-120-1993>, 1993.

705 Harvey, A. H.: Properties of Ice and Supercooled Water, in: *CRC Handbook of Chemistry and Physics*  
706 (97th ed.), edited by Haynes, W. Lide, D. R. and Bruno, T., Boca Raton, FL: CRC Press., 2019.

707 Häuselmann, P., Granger, D.E., Jeannin, P.-Y., and Lauritzen, S.-E.: Abrupt glacial valley incision at  
708 0.8 Ma dated from cave deposits in Switzerland. *Geology*, 35, 143–146,  
709 <https://doi.org/10.1130/G23094A>, 2007.

710 Herman, F., and Braun, J.: Evolution of the glacial landscape of the Southern Alps of New Zealand:  
711 insights from a glacial erosion model. *J. Geophys. Res.* 113, F02009,  
712 <https://doi.org/10.1029/2007JF000807>, 2008.

713 Herman, F., Beaud, F., Champagnac, J.-D., Lemieux, J.-M., and Sternai, P.: Glacial hydrology and  
714 erosion patterns: a mechanism for carving glacial valleys. *Earth Planet. Sci. Lett.* 310, 498–508,  
715 <https://doi.org/10.1016/j.epsl.2011.08.022>, 2011.

716 Herman, F., Beyssac, O., Brughelli, M., Lane, S.N., Leprince, S., Adatte, T., Lin, J.Y.Y., Avouac, J.-  
717 P., and Cox, S.C.: Erosion by an Alpine glacier. *Science*, 350, 193–195.  
718 <https://doi.org/10.1126/science.aab2386>, 2015.

719 Hinderer, M. Late Quaternary denudation of the Alps, valley and lake fillings and modern river loads.  
720 *Geodinamica Acta*, 14, 231–263, <https://doi.org/10.1080/09853111.2001.11432446>, 2001.

721 Hooke, R.L., and Pohjola, V.A.: Hydrology of a segment of a glacier situated in an overdeepening,  
722 Storglaciären, Sweden. *J. Glaciol.*, 40, 140–148, <https://doi.org/10.3189/S0022143000003919>,  
723 1994.

724 Isenschmid, C.: Die Grenze Untere Süswassermolasse/Obere Meeremolasse als Schlüssel zur Tektonik  
725 in der Region Bern. *Mitt. Natf. Ges. Bern*, 76, 108–133, 2019.

726 Jansen, J.D., Codilean, A.T., Stroeven, A.P., Fabel, D., Hättestrand, C., Kleman, J., Harbor, J.M.,  
727 Heyman, J., Kubik, P.W., and Xu, S.: Inner gorges cut by subglacial meltwater during  
728 Fennoscandian ice sheet decay. *Nat. Comm.*, 5, 3815, <https://doi.org/10.1038/ncomms4815>,  
729 2014.

730 Jørgensen, F., and Sandersen, P.B.E.: Buried and open tunnel valleys in Denmark—erosion beneath  
731 multiple ice sheets. *Quat. Sci. Rev.*, 25, 1339–1363,  
732 <https://doi.org/10.1016/j.quascirev.2005.11.006>, 2006.

733 Jordan, P.: Analysis of overdeepened valleys using the digital elevation model of the bedrock surface  
734 of northern Switzerland. *Swiss J. Geosci.*, 103, 375–384, <https://doi.org/10.1007/s00015-010-0043-z>, 2010.

735

736 Kehew, A.E., Piotrowski, J.A., and Jørgensen, F.: Tunnel valleys: concepts and controversies – a  
737 review. *Earth-Sci. Rev.* 113, 33–58, <https://doi.org/10.1016/j.earscirev.2012.02.002>, 2012.

738 Kellerhals, P., and Häfeli, C.: Brunnenbohrung Münsingen. Geologische Dokumentation des Kantons  
739 Bern, WEA-Geologie, Beilage Nr. 2, 7 pp, 1984.

740 Kissling, E., Schwendener, H.: The Quaternary sedimentary fill of some Alpine valleys by gravity  
741 modeling. *Eclogae Geol. Helv.*, 83, 311–321, 1990.

742 Koutsodendris, A., Pross, J., Müller, U. C., Brauer, A., Fletcher, W. J., Kühl, N., Kirilova, E., Verhagen,  
743 F. T., Lücke, A., and Lotter, A. F.: A short-term climate oscillation during the Holsteinian  
744 interglacial (MIS 11c): An analogy to the 8.2ka climatic event?, *Global Planet. Chang.*, 92–93,  
745 224–235, <https://doi.org/10.1016/j.gloplacha.2012.05.011>, 2012.

746 Krohn, C. F., Larsen, N. K., Kronborg, C., Nielsen, O. B., and Knudsen, K.: L. Litho- and  
747 chronostratigraphy of the Late Weichselian in Vendyssel, northern Denmark, with special  
748 emphasis on tunnel-valley infill in relation to a receding ice margin. *Boreas*, 38, 811–833,  
749 <https://doi.org/10.1111/j.1502-3885.2009.00104.x>, 2009.

750 Kühni, A., and Pfiffner, O.A.: The relief of the Swiss Alps and adjacent areas and its relation to lithology  
751 and structure: topographic analysis from a 250-m DEM. *Geomorphology*, 41, 285–307,  
752 [https://doi.org/10.1016/S0169-555X\(01\)00060-5](https://doi.org/10.1016/S0169-555X(01)00060-5), 2001.

753 Liebl, M., Robl, J., Hergarten, S., Egholm, D.L., and Stüwe, K.: Modeling large-scale landform  
754 evolution with a stream power law for glacial erosion (OpenLEM v37): benchmarking  
755 experiments against a more process-based description of ice flow (iSOSIA v3.4.3). *Geosci.*  
756 *Model Dev.*, 16, 1315–1343, <https://doi.org/10.5194/gmd-16-1315-2023>, 2023.

757 Lloyd, C., Clark, C.D., and Swift, D.A.: The effect of valley confluence and bedrock geology upon the  
758 location and depth of glacial overdeepenings. *Geogr. Ann.: Series A, Phys. Geogr.*,  
759 <https://doi.org/10.1080/04353676.2023.2217047>, 2023.

760 Lohrberg, A., Schneider von Deimling, J., Grob, H., Lenz, K.-F., and Krastel, S.: Tunnel valleys in the  
761 southeastern North Sea: More data, more complexity. *E&G Quat. Sci. J.*, 71, 267–274,  
762 <https://doi.org/10.5194/egqsj-71-267-2022>, 2022.

763 Magrani, F., Valla, P.G., Gribenski, N., and Serra, E.: Glacial overdeepening in the Swiss Alps and  
764 foreland: Spatial distribution and morphometrics. *Quat. Sci. Rev.*, 243, 106483,  
765 <https://doi.org/10.1016/j.quascirev.2020.106483>, 2020.

766 Magrani, F., Valla, P.G., and Egholm, D.: Modelling alpine glacier geometry and subglacial erosion  
767 patterns in response to contrasting climatic forcing. *Earth Surf. Process. Landf.*, 47, 1954–1072,  
768 <https://doi.org/10.1002/esp.5302>, 2022.

769 Moreau, J., Huuse, M., Janszen, A., van der Vegt, P., Gibbard, P. L., and Moscriello, A.: The  
770 glaciogenic unconformity of the southern North Sea. *Geol. Soc. London Spec. Publ.*, 368, 99,  
771 <https://doi.org/10.1144/SP368.5>, 2012.

772 Montgomery, D. R., and Korup, O.: Preservation of inner gorges through repeated Alpine glaciations.  
773 Nat. Geosci., 4, 62-67, <https://doi.org/10.1038/Ngeo1030>, 2011.

774 Nagy, D.: The gravitational attraction of a right rectangular prism. *Geophyscis*, 31, 362–271, 1996.

775 Nishiyama, R., Ariga, A., Ariga, T., Lechmann, A., Mair, D., Pistillo, C., Scampoli, P., Valla, P.G.,  
776 Vladymyrov, M., Ereditato, A., and Schlunegger, F.: Bedrock sculpting under an active alpine  
777 glacier revealed from cosmic-ray muon radiography. *Sci. Rep.*, 9, 6970,  
778 <https://doi.org/10.1038/s41598-019-43527-6>, 2019.

779 Olivier, R., Dumont, B., and Klingele, E.: Carte gravimétrique de la Suisse (Anomalies de Bouguer)  
780 1:500'000. Bundesamt für Landestopographie swisstopo,  
781 <https://opendata.swiss/fr/dataset/schwerekarte-der-schweiz-bouguer-anomalien-1-500000>,  
782 2008, 2011.

783 Ottesen, D., Stewart, M., Brönnner, M., and Batchelor, C. L.: Tunnel valleys of the central and northern  
784 North Sea (56°N to 62°N): Distribution and characteristics, *Mar. Geol.*, 425, 106199,  
785 <https://doi.org/10.1016/j.margeo.2020.106199>, 2020.

786 Patton, H., Swift, D. A., Clark, C. D., Livingstone, S. J., and Cook, S. J.: Distribution and characteristics  
787 of overdeepenings beneath the Greenland and Antarctic ice sheets: Implications for  
788 overdeepening origin and evolution. *Quat. Sci. Rev.*, 148, 128–145,  
789 <https://doi.org/10.1016/j.quascirev.2016.07.012>, 2016.

790 Pedersen, V.K., and Egholm, D.L.: Glaciations in response to climate variations preconditioned by  
791 evolving topography. *Nature*, 493, 206-201, <https://doi.org/10.1038/nature11786>, 2013.

792 Perrouy, S., Moussirou, B., Martinod, J., Banvalot, S., Carretier, S., Gabalda, G., Monod, B., Hérail,  
793 G., Regard, V., and Remy, D.: Geometry of two glacial valleys in the northern Pyrenees  
794 estimated using gravity data, *Comptes Rendus Geosci.*, 347, 13–23,  
795 <https://doi.org/10.1016/j.crte.2015.01.002>, 2015.

796 Piotrowski, J.A.: Subglacial hydrology in north-western Germany during the last glaciation:  
797 Groundwater flow, tunnel valleys and hydrological cycles. *Quat. Sci. Rev.*, 16, 169-185,  
798 [https://doi.org/10.1016/S0277-3791\(96\)00046-7](https://doi.org/10.1016/S0277-3791(96)00046-7), 1997.

799 Platt, N., and Keller, B.: Distal alluvial deposits in a foreland basin setting – the Lower Freshwater  
800 Molasse (Lower Miocene), Switzerland: sedimentology, architecture and palaeosols.  
801 *Sedimentology*, 39, 545-565, <https://doi.org/10.1111/j.1365-3091.1992.tb02136.x>, 1992.

802 Preusser, F., and Schlüchter, C. Dates from an important early Late Pleistocene ice advance in the Aare  
803 valley, Switzerland. *Eclogae Geol. Helv.*, 97, 245–253, [https://doi.org/10.1007/s00015-004-](https://doi.org/10.1007/s00015-004-1119-4)  
804 1119-4, 2004.

805 Preusser, F., Drescher-Schneider, R., Fiebig, M., and Schlüchter, C.: Re-interpretation of the Meikirch  
806 pollen record, Swiss Alpine Foreland, and implications for Middle Pleistocene  
807 chronostratigraphy. *J. Quat. Sci.*, 20., 607-620, <https://doi.org/10.1002/jqs.930>, 2005.

808 Preusser, F., Reitner, J. M., and Schlüchter, C.: Distribution, geometry, age and origin of overdeepened  
809 valleys and basins in the Alps and their foreland. *Swiss J. Geosci.*, 103, 407–426,  
810 <https://doi.org/10.1007/s00015-010-0044-y>, 2010.

811 Preusser, F., Graf, H. R., Keller, O., Krayss, E., and Schlüchter, C.: Quaternary glaciation history of  
812 Northern Switzerland. *E&G Quat. Sci. J.*, 60, 282–305, <https://doi.org/10.3285/eg.60.2-3.06>,  
813 2011.

814 Reber, R., and Schlunegger, F.: Unravelling the moisture sources of the Alpine glaciers using tunnel  
815 valleys as constraints. *Terra Nova*, 28, 202–211, <https://doi.org/10.1111/ter.12211>, 2016.

816 Reitner, J.M., Gruber, W., Römer, A., and Morawetz, R.: Alpine overdeepenings and paleo-ice flow  
817 changes: an integrated geophysical-sedimentological case study from Tyrol (Austria). *Swiss J.*  
818 *Geosci.*, 103, 385–405, <https://doi.org/10.1007/s00015-010-0046-9>, 2010.

819 Roger, S., Féraud, G., de Beaulieu, J.-L., Thouveny, N., Coulon, Ch., Choucem., J.J., Andrieu, V. and  
820 Williams, T.: <sup>40</sup>Ar/<sup>39</sup>Ar dating on tephra of the Velay maars (France): implications for the  
821 Late Pleistocene proxy-climatic record. *Earth Planet Sci. Lett.*, 170: 287–299, 1999.

822 Ross, N., Siegert, M.J., Woodward, J., Smith, A.M., Corr, H.F.J., Bentley, M.J., Hindsmarsh, R.C.A.,  
823 King, E.C., and Rivera, A.: Holocene stability of the Amundsen-Weddell ice divide, West  
824 Antarctica. *Geology*, 39, 935–938, <https://doi.org/10.1130/G31920>, 2011.

825 Rosselli, A., and Raymond, O. : Modélisation gravimétrique 2.5D et cartes des isohypses au 1:100'000  
826 du substratum rocheux de la Vallée du Rhône entre Villeneuve et Brig (Suisse). *Eclogae Geol.*  
827 *Helv.*, 96, 399–423, 2003.

828 Schaller, S., Büchi, M.W., Schuster, B., and Anselmetti, F.: Drilling into a deep buried valley (ICDP  
829 DOVE): a 252 m long sediment succession from a glacial overdeepening in northwestern  
830 Switzerland. *Sci. Drill.*, 32, 27–42, <https://doi.org/10.5194/sd-32-27-2023>, 2023.

831 Schläfli, P., Gobet, E., van Leeuwen, J.F.N., Vescovi, E., Schwenk, M.A., Bandou, D., Douillet, G.A.,  
832 Schlunegger, F., and Tinner, W.: Palynological investigations reveal Eemian interglacial  
833 vegetation dynamics at Spiezberg, Bernese Alps, Switzerland. *Quat. Sci. Rev.*, 263, 106975,  
834 <https://doi.org/10.1016/j.quascirev.2021.106975>, 2021.

835 Schlüchter, C.: Thalgut: ein umfassendes eiszeitstratigraphisches Referenzprofil im nördlichen  
836 Alpenvorland. *Eclogae geol. Helv.*, 82, 277–284, 1989.

837 Schlüchter, C. The Swiss glacial record – a schematic summary. *Develop. Quat. Sci.*, 2, 413–418,  
838 [https://doi.org/10.1016/S1571-0866\(04\)80092-7](https://doi.org/10.1016/S1571-0866(04)80092-7), 2004.

839 Schlunegger, F., and Garefalakis, P.: Einführung in die Sedimentologie, Schweizerbart, Stuttgart,  
840 [www.schweizerbart.de/9783510655397](http://www.schweizerbart.de/9783510655397), 2023.

841 Schwenk, M., Schläfli, P., Bandou, D., Gribenski, N., Douillet, G., and Schlunegger, F.: From glacial  
842 erosion to basin overfill: A 240 m-thick overdeepening-fill sequence in Bern. Switzerland. *Sci.*  
843 *Drill.*, 30, 17–42, <https://doi.org/10.5194/sd-30-17-2022>, 2022a.

844 Schwenk, M. A., Stutenbecker, L., Schläfli, P., Bandou, D., and Schlunegger, F.: Two glaciers and one  
845 sedimentary sink: The competing role of the Aare and the Valais glaciers in filling an  
846 overdeepened trough inferred from provenance analysis. *E&G Quat. Sci. J.*, 71, 163–190,  
847 <https://doi.org/10.5194/egqsj-71-163-2022>, 2022b.

848 Stäger, D., Labhart, T., Della Valle, G., Tröhler, B., Schwarz, H., Gisler, C., Rathmayr, B. and  
849 Wiederkehr, M. Blatt 1210 Innertkirchen. *Geol. Atlas Schweiz 1:25'000, Karte 167, Swisstopo*,  
850 2020.

851 Steinemann, O., Ivy-Ochs, S., Hippe, K., Christl, M., Naghipour, N., and Synal, H.-A.: Glacial erosion  
852 by the Trift glacier (Switzerland): Deciphering the development of riegels, rock basins and  
853 gorges. *Geomorphology*, 375, 107533, <https://doi.org/10.1016/j.geomorph.2020.107533>, 2021.

854 Stewart, M.A., and Lonergan, L.: Seven glacial cycles in the middle-late Pleistocene of northwest  
855 Europe: geomorphic evidence from buried tunnel valleys. *Geology* 39, 283-286,  
856 <https://doi.org/10.1130/G31631.1>, 2011.

857 Stewart, M.A., Lonergan, L. and Hampson, G.: 3D seismic analysis of buried tunnel valleys in the  
858 central North Sea: tunnel valley-fill sedimentary architecture, in: *Glaciogenic Reservoirs and*  
859 *Hydrocarbon Systems*, edited by: Huuse, M., Redfern, J., Le Heron, D.P., Dixon, R.J., and  
860 Moscariello, A.. *Geol. Soc. London Spec. Publ.*, 368, 173-183,  
861 <http://dx.doi.org/10.1144/SP368.9>, 2013.

862 Valla, P.G., van der Beek, P.A., and Carcaillet, J.: Dating bedrock gorge incision in the French Western  
863 Alps (Ecrins-Pelvoux massif) using cosmogenic <sup>10</sup>Be. *Terra Nova*, 22, 18-25,  
864 <https://doi.org/10.1111/j.1365-3121.2009.00911.x>, 2010.

865 Valla, P., Shuster, D.L., and van der Beek, P.A.: Significant increase in relief of the European Alps  
866 during mid-Pleistocene glaciations. *Nat. Geosci.*, 4, 688-692,  
867 <https://doi.org/10.1038/ngeo1242>, 2011.

868 Welten, M.: Pollenanalytische Untersuchungen im jüngeren Quartär des nördlichen Alpenvorlandes der  
869 Schweiz. *Beitr. Geol. Karte Schweiz*, 156, 174 pp., 1982.

870 Welten, M.: Neue pollenanalytische Ergebnisse über das jüngere Quartär des nördlichen  
871 Alpenvorlandes der Schweiz (Mittel- und Jungpleistozän). *Beitr. Geol. Karte Schweiz*, 162, 9-  
872 40, 1988.

873 Wright, H. E.: Tunnel valleys, glacial surges, and subglacial hydrology of the Superior Lobe, 340  
874 Minnesota. *Mem. Geol. Soc. Amer.*, 136, 251-276, <https://doi.org/10.1130/MEM136-p251>,  
875 1973.

876 Zwahlen, P., Tinner, W. and Vescovi, E.: Ein neues EEM-zeitliches Umweltarchiv am Spiezberg  
877 (Schweizer Alpen) im Kontext der mittel- und spätpleistozänen Landschaftsentwicklung. *Mitt.*  
878 *Naturf. Ges. Bern* 78, 92–121, 2021.